2023

Characterization of Sphingosine-1-Phosphate Receptor Expression and Functionality in Niemann-Pick Type C Disease

Nathaniel-David I. Dizon
Virginia Commonwealth University

Characterization of Sphingosine-1-Phosphate Receptor Expression and Functionality in Niemann-Pick Type C Disease

A thesis submitted in partial fulfillment of the requirements for the degree of Master of Science in Biology at Virginia Commonwealth University

By:

Nathaniel-David I. Dizon

B.S. Biology, Virginia Commonwealth University, 2015

P.I. Dr. Jason Newton, PhD

Assistant Professor, Department of Biology

Virginia Commonwealth University

Richmond, Virginia

April 2023

Acknowledgements

I would like to acknowledge and give thanks to my supervisor Dr. Jason Newton who made this work possible and whose guidance carried me through my thesis project. I would also like to give thanks to my committee members Dr. Santiago Lima, Dr. Derek Prosser, and Dr. Sarah Rothschild whose advice, comments, and suggestions were a great help through this tough and rewarding challenge.

I would also like to acknowledge my fellow lab mates, especially Elizabeth Malaugh, Isaiah Klimek, Amanda Stocker, Christian Clemons, Betsy Gulliksen, and Noriko Senaratne whose help and company were invaluable to my project. Additionally, I want to give thanks to the Graduate Organization of Biology Students (GOBS) who offered a source of support and camaraderie amongst the biology master's students.

I would like to thank my brother, Nikko Dizon, my parents Nick and Donna Dizon, and my aunts Marilene Capellan and Christine Idquival, for the love, support, and encouragement they gave me as I completed this academic journey. Lastly, I'd like to recognize my friends Ryan Tolliver, Michael Ventura, and Samantha McLean whose encouragement and company kept my spirits and motivation high during this process.

Table of Contents

List of Tables and Figures

Abbreviations

Abbreviation	Definition
NPC	Niemann-Pick Type C Disease
LDL	Low-Density Lipoprotein
LE/L	Late Endosome/Lysosome
ER	Endoplasmic Reticulum
SphK1	Sphingosine Kinase 1
SphK2	Sphingosine Kinase 2
S1P	Sphingoine-1-Phosphate
SPT	Serine-Palmitoyl CoA Transferase
3-KSR	3-Ketosphinganine Reductase
CerS (1-6)	Ceramide Synthase (1-6)
DES	Ceramide Desaturase
CERT	Ceramide Transfer Protein
SPL	S1P Lyase
CDase	Ceramidase
aCDase	Acidic Ceramidase
C1P	Ceramide-1-Phosphate
TNF-α	Tumor Necrosis Factor Alpha
NF-κB	Nuclear Factor Kappa B
ATP	Adenosine Tri-Phosphate
ABC	ATP-Binding Cassette
Spn2	Spinster 2
GPCR	G-Protein Coupled Receptor
S1PR (1-5)	S1P Receptor (1-5)
PI3K or AKT	Phosphoinositide-3-Kinase
MAPK or ERK (1-2)	Mitogen-Activated Protein Kinase (1-2)
ROCK	Rho-Rho Kinase
mRNA	Messenger RNA
qPCR	Quantitative Polymerase Chain Reaction
DMEM	Dulbeco's Modified Eagle Medium
FBS	Fetal Bovine Serum
DEPC-Water	Diethyl Pyrocarbonate Treated Water
cDNA	Complimentary DNA
ddH_2O	Double Distilled Water
PBS	Phosphate Buffered Saline
SDS	Sodium Dodecyl Sulfate
PAGE	Polyacrylamide Gel Electrophoresis
EDTA	Ethylenediaminetetraacetic Acid
DTT	Dithiothreitol
Tris-HCl	Tris(hydroxymethyl)aminomethane Hydrochloride
BSA	Bovine Serum Albumin
TBS	Tris Buffered Saline
TBS-T	Tris-Buffered Saline with Tween-20
GAPDH	Glyceraldehyde-3-phosphate dehydrogenase
TNE	Tris-NaCl-EDTA
DMSO	Dimethyl Sulfoxide

Abstract

Niemann Pick Type C (NPC) is a recessively inherited lysosomal storage disorder for which there is currently no major treatment. It is widely acknowledged that the pathology of NPC is caused by a trafficking defect which leads to an accumulation of cholesterol in the late endosome/lysosome compartment (LE/L). In addition to cholesterol, multiple species of sphingolipids are observed to accumulate as well in the LE/L. Specifically, an accumulation of sphingosine is observed in NPC disease and is likely attributed to the decreased activity of an enzyme, sphingosine kinase 1 (SphK1), which is responsible for phosphorylating sphingosine into an important pro-survival signaling molecule called sphingosine-1-phosphate (S1P). Previous work has shown that either the overexpression of SphK1 or the addition of nM concentrations of S1P can correct deficiencies observed in NPC models, however the impact of decreased S1P and the signaling cascades they regulate via the activation of 1 of 5 transmembrane S1P receptors are incompletely described. Accordingly, we sought to determine the baseline levels of the S1P receptors (S1PRs) in *NPC1* mutant and *NPC1* knockout (KO) cells, as well as the biological consequences of the dysregulated expression of the S1PR's in NPC disease. In this study, a significant increase in S1PR1, and S1PR2 mRNA was observed via reverse transcriptase (RT) qPCR in *NPC1* KO cells, as well as in mouse brain and liver tissue. Conversely, western blot analysis of *NPC1* KO HeLa cells shows no difference in protein expression of S1PR1 or S1PR2. Following gene and protein expression analysis, the cellular localization of S1PR1 and S1PR2 were analyzed via fluorescence microscopy. Initial results showed that *NPC1* KO cells have no change in transmembrane S1PR1, but a decreased amount of transmembrane S1PR2. The functionality of S1PR1 and S1PR2 was assessed by treating *NPC1* KO cells with agonist and antagonist drugs for S1PR1 and S1PR2 and utilizing western blots to qualitatively and quantitatively analyze the presence and activation of the phosphoinositide-3-kinase (AKT) and mitogen-activated protein kinase (ERK) signaling cascades. Initial results indicated that *NPC1* KO cells treated with CYM-5520 (S1PR2 agonist) demonstrated a significant decrease in activation of the AKT pathway, and that treatment with JTE-013 (S1PR2 antagonist) restored activation of the AKT pathway. These results indicate that S1PR2 blockage may provide potential therapeutic benefits, however further studies are needed to elucidate specific molecular interactions involved in the regulation of the AKT pathway by S1PR2.

Introduction

I.1 Niemann Pick Type C Disease

Niemann Pick Type C disease (NPC) is a recessively inherited lysosomal storage disorder that results from mutations in either the *NPC1* or *NPC2* genes. Under normal circumstances, it is suggested that low-density lipoprotein (LDL)-derived cholesterol is internalized and hydrolyzed into unesterified cholesterol in the late endosome/lysosome compartment (LE/L). Once unesterified, cholesterol can bind to cytosolic *NPC2* and orient the molecule to optimally transfer to *NPC1*, which traffics the cholesterol molecule out of the LE/L either to the cell surface or the endoplasmic reticulum (ER) [1]–[5]. Being as *NPC1* and *NPC2* work in tandem, loss of function in either the *NPC1* or *NPC2* proteins results in an accumulation of unesterified cholesterol and sphingolipids inside the LE/L [6]–[8].

About 95% of the individuals who are afflicted with NPC disease have a mutation on the *NPC1* gene, and the remaining patients have a mutation on the *NPC2* gene [1], [9], [10]. It has been estimated that the minimum incidence of NPC disease is about 1 per 120,000 live births [7], [8], [10]. Typically, NPC disease presents itself during early childhood (2 – 8 years old), however it can also present during both the perinatal period (0 – 24 months old) or during adulthood with an earlier age of onset being correlated with a poorer prognosis and increased disease severity [8]. Patients with NPC disease eventually develop progressive and fatal neurological degradation, often experiencing symptoms such as cerebellar ataxia, dysphagia, and dementia [11]–[13]. Adult-onset subtypes of NPC have also been reported to present with psychiatric symptoms that phenocopy other neurodegenerative diseases such as Alzheimer's, Wilson's, or Parkinson's diseases [10], [14]–[16]. Due to the clinical heterogeneity of NPC,

diagnosis of this disease can be challenging, and the prevalence of NPC can be higher than estimated as a result of these misdiagnoses [10].

Out of roughly 50 lysosomal storage diseases categorized by lipid accumulation in the endo-lysosomal compartment, NPC disease is sub-categorized as a type of sphingolipidosis [13], [17]. Sphingolipidoses are characterized by their defective degradation and accumulation of sphingolipids. In the case of NPC disease, one enzyme that has been shown to have decreased activity is one of two sphingosine kinase isoforms, sphingosine kinase 1 (SphK1), which is responsible for producing an important and potent bioactive signaling molecule sphingosine-1-phosphate (S1P) from its precursor molecule sphingosine [18], [19].

I.2 Sphingolipids

Although originally thought to be an inert structural component of the plasma membrane, sphingolipids are now recognized to be a group of both structural and functional lipids. Sphingolipids on the plasma membrane can exert biological functions that affect the properties of plasma membrane associated proteins such as growth factor receptors and adhesion molecules [16]. In addition to their membrane functions, sphingolipids are also responsible for regulating a wide variety of critical cellular processes such as cell proliferation, survivability, and apoptosis [20], [21]. Notable among the sphingolipids are two bioactive signaling molecules that are key contributors to these processes: ceramide and S1P.

The common structural component of all sphingolipids is the presence of sphingosine, an 18-carbon amino-alcohol that serves as the sphingoid backbone of sphingolipids [22], [23] **(Figure 1**). When sphingosine molecules are amide-linked with other fatty acids they create a ceramide molecule. Ceramide is considered to be the center of the sphingolipid biosynthesis

pathway as it serves as the branching point for the biosynthesis of multiple types of sphingolipids such as glycosphingolipids and sphingomyelin [24].

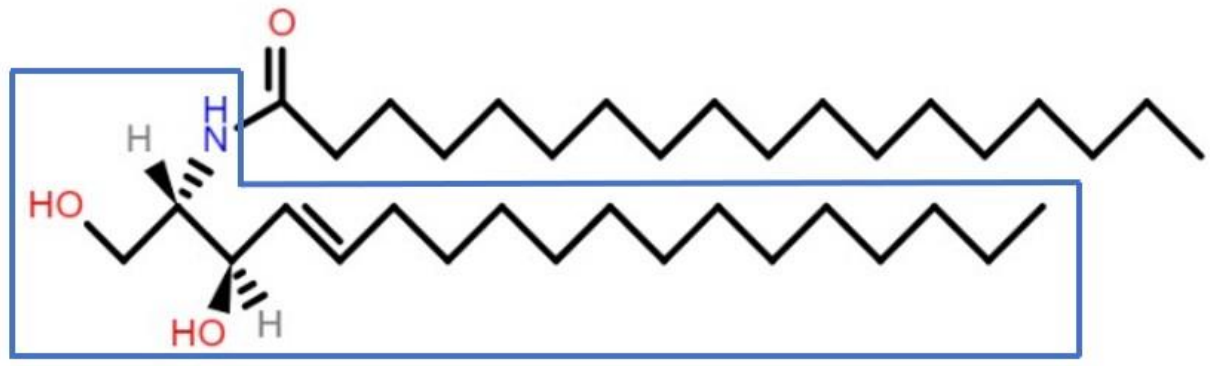

Figure 1: Structure of C18 Ceramide – Image Created Using JChemPaint

Ceramide serves as the branching point for the synthesis of more complex sphingolipids such as sphingomyelin and glucosylceramide. Its structure consists of a sphingoid backbone (sphingosine boxed in blue), that is amide-linked to a fatty acyl-CoA group whose structure can vary dependent on the acyl chain length and presence of double bonds. Complex sphingolipids are formed when different head groups link to the primary hydroxyl group of ceramide molecules.

I.2.1 Sphingolipid Metabolism

Ceramides are the central molecule in the sphingolipid biosynthesis pathway and can be synthesized by either the *de novo* pathway or salvage pathway. The *de novo* pathway **(Figure 2)** is a four-step process that takes place at the cytosolic face of the endoplasmic reticulum and begins when the amino acid serine and palmitoyl-CoA are condensed by serine-palmitoyl CoA transferase (SPT) to create 3-ketosphinganine [25]. In the next step of the *de novo* pathway, 3-ketosphinganine is reduced into sphinganine by 3-ketosphinganine reductase (3-KSR). Sphinganine is then further reduced by one of six ceramide synthase isoforms (CerS1-6) into dihydro-ceramide. In the last step of the *de novo* pathway, dihydro-ceramide is desaturated by

ceramide desaturase (DES) to produce the central molecule of the sphingolipid biosynthesis pathway, ceramide [25]. Once ceramide is produced, it is transported to the Golgi complex through vesicular ER-to-Golgi trafficking or via a separate, non-vesicular shuttling mechanism by ceramide transfer protein (CERT) where it can be modified to form ceramide-1-phosphate (C1P) and various complex sphingolipids such as sphingomyelin and glycosphingolipids. Alternatively, ceramide can be broken down into sphingosine and free fatty acids by ceramidases in the ER [25]–[27] **(Figure 2)**.

Sphingolipid catabolism is dependent on the phosphorylation of sphingosine into S1P by one of two sphingosine kinase isoforms (SphK1 or SphK2) [28], [29]. In the final step of sphingolipid catabolism, S1P is irreversibly degraded by S1P Lyase (SPL) into hexadecenal and ethanolamine phosphate [30], [31] **(Figure 2)**. Alternatively, S1P can be dephosphorylated back into sphingosine, which can be re-acylated back to ceramide via the pathway discussed below [25], [32].

I.2.2 Ceramide Synthesis via the Salvage Pathway

Along with the *de* novo pathway, ceramide can also be produced via the salvage pathway in acidic compartments such as the LE/L [33] **(Figure 2)**. The salvage pathway involves the recycling of sphingosine and is estimated to contribute between 50% to 90% of sphingolipid biosynthesis [33]–[35]. During the salvage pathway, complex sphingolipids, mainly sphingomyelin, are converted back into ceramide by their respective enzymes (e.g. sphingomyelinases). As ceramide molecules are not able to leave the LE/L, they need to be further hydrolyzed by acid ceramidase (aCDase) in order to catabolize ceramide into sphingosine and free fatty acids [13], [33], [36]. The sphingosine molecules produced by this reaction are

transported out of the LE/L to the ER by a currently uncharacterized mechanism and can re-enter the metabolic pathway to be utilized by one of six CerS isoforms to form ceramide, or by one of two SphK isoforms to form S1P [33].

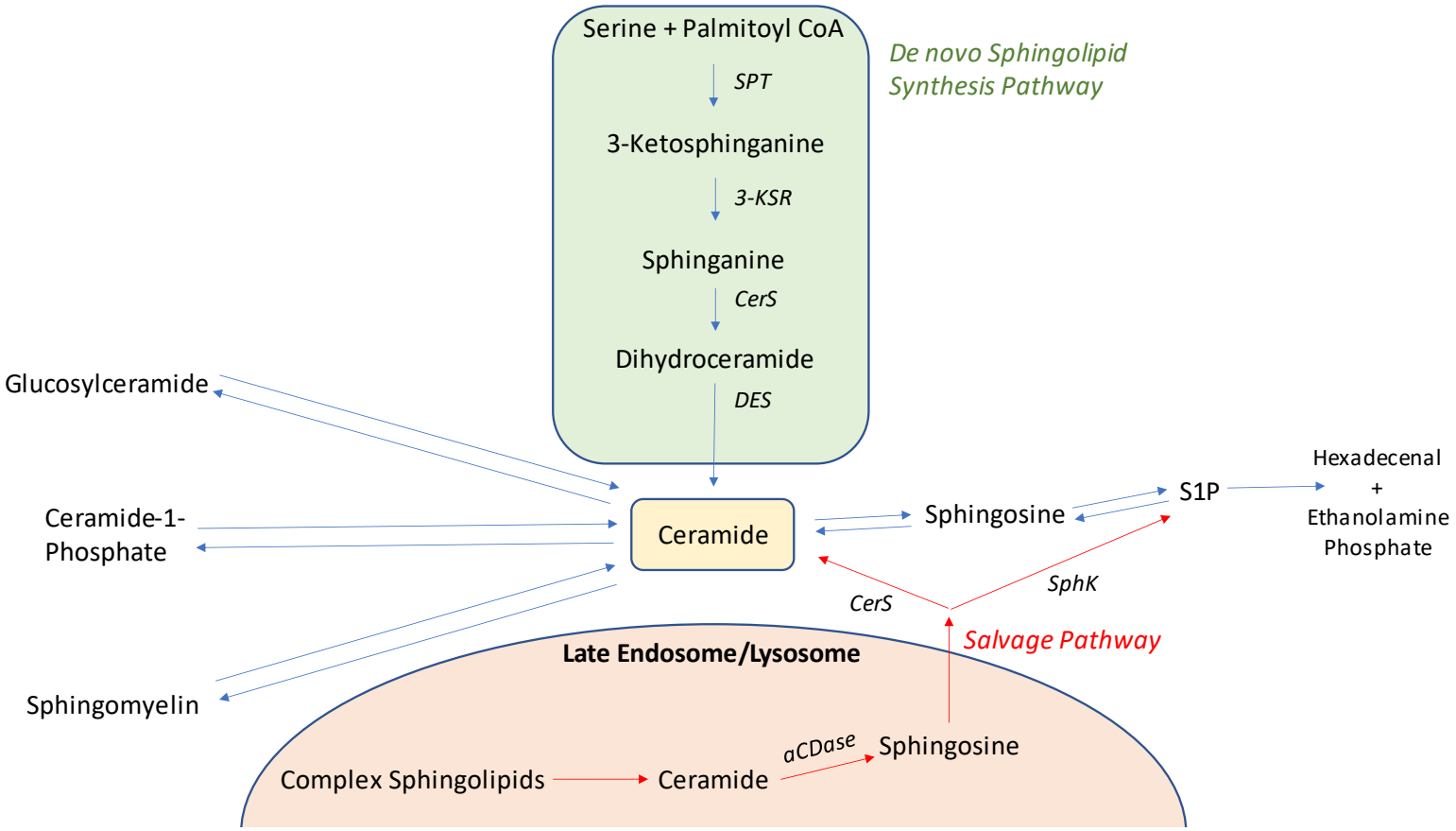

Figure 2: Sphingolipid Metabolic Pathways

Ceramide can be synthesized through either the *De novo* pathway, or the Salvage pathway. The *de novo* pathway (Green) is a four-step process that begins with the condensation of Serine and Palmitoyl CoA. The Salvage pathway (Red) breaks down complex sphingolipids back into ceramide, which is further catabolized into sphingosine by acid ceramidase. Unlike ceramide, sphingosine can leave the LE/L and re-enter the metabolic pathway.

I.3 Sphingolipid Signaling

Sphingolipid signaling is accomplished via an important subset of bioactive signaling molecules comprised of ceramide, sphingosine, and their respective phosphorylated metabolites C1P and S1P. Perhaps the best characterized among the sphingolipid signaling modules is the intracellular balance of ceramide and S1P, often referred to as the sphingolipid rheostat, which dictates that the relative levels of ceramide and S1P are responsible for cellular fate decisions **(Figure 3)** [32]. Ceramide is known to mediate antiproliferative actions such as apoptosis and cell cycle arrest whereas S1P is a positive regulator of cell proliferation, motility, and survival [16], [20], [37]–[40]. As such, maintaining homeostasis of these two signaling molecules is necessary for normal functioning cells [20]. Dysregulation of the enzymes that create ceramide or S1P can result in the abnormal function of cells.

I.3.1 Sphingosine-1-Phosphate

S1P is produced when sphingosine is phosphorylated by one of two sphingosine kinase isoforms: SphK1 located in the cytosol or SphK2 located in the nucleus or mitochondria [41]. S1P is responsible for regulating a diverse variety of biological functions through intracellular and extracellular signaling cascades. For example, intracellular S1P plays a vital role in the regulation of Tumor Necrosis Factor Alpha/Nuclear Factor Kappa B (TNF-α/NF-κB) signaling pathway through regulation of the ubiquitination activity to the E3 ligase TNF Receptor Associated Factor 2 (TRAF2) [42]–[44]. Conversely, S1P can be actively transported into the extracellular environment via ATP-binding cassette (*ABC*) transporters or Spinster 2 (*Spns2*), where they can regulate different physiological functions by activating one of five G-coupled protein receptors (GCPR) located in the plasma membrane: S1P Receptor 1 (S1PR1), S1PR2,

S1PR3, S1PR4, and S1PR5 [45]–[48]. This action is described as “inside-out” signaling of S1P **(Figure 3)**.

Each of the five S1P receptors have their own distinct downstream processes that they can regulate such as the phosphoinositide-3-kinase (PI3K or AKT) pathway, mitogen-activated protein kinase (MAPK or ERK) signaling pathway, and Rho-Rho kinase (ROCK) pathway **(Figure 4)** [49]–[53]. Further, the expression levels of the S1P receptors differs by tissue type. S1PR1 is commonly expressed across various tissue types and is a GCPR that exclusively couples with $G_{\alpha i/\alpha o}$ proteins. S1PR2 and S1PR3 are also commonly expressed across tissue types and can couple with $G_{\alpha i/\alpha o}$, $G_{\alpha q}$, and $G_{\alpha 12/\alpha 13}$ proteins. S1PR4 is mainly expressed on lymphoid tissue and couples with $G_{\alpha i/\alpha o}$ and $G_{\alpha 12/\alpha 13}$ proteins. S1PR5 is mainly expressed in the brain, spleen, and bone marrow and can also couple with $G_{\alpha i/\alpha o}$ and $G_{\alpha 12/\alpha 13}$ proteins [45], [47], [54].

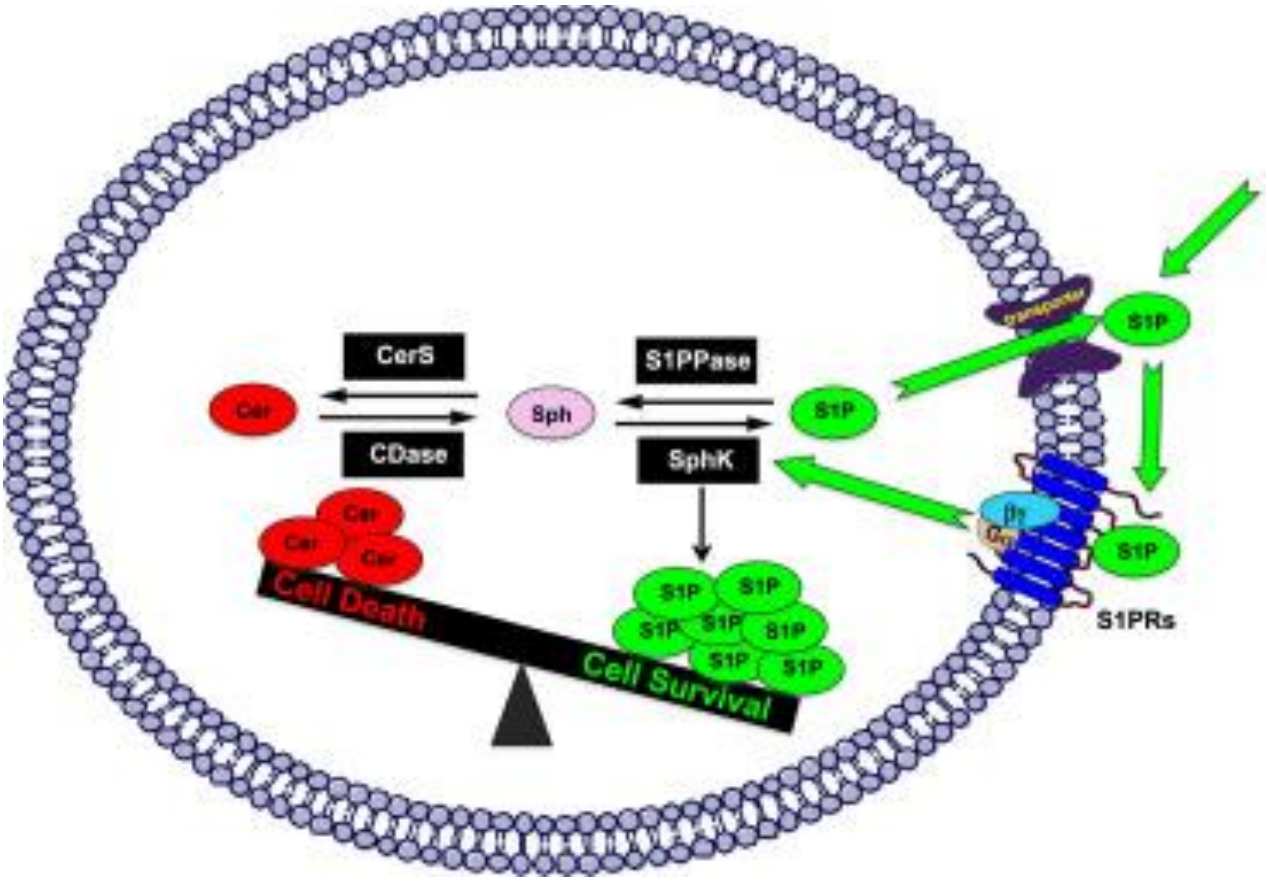

Figure 3: The Sphingolipid Rheostat – Adapted from Newton, Lima, Maceyka, and Spiegel, 2015

Schematic that illustrates key enzymes that are responsible for regulating ceramide and S1P inside the cell. Additionally, this schematic illustrates the "inside-out" signaling action of S1P, and its influence on the sphingolipid rheostat.

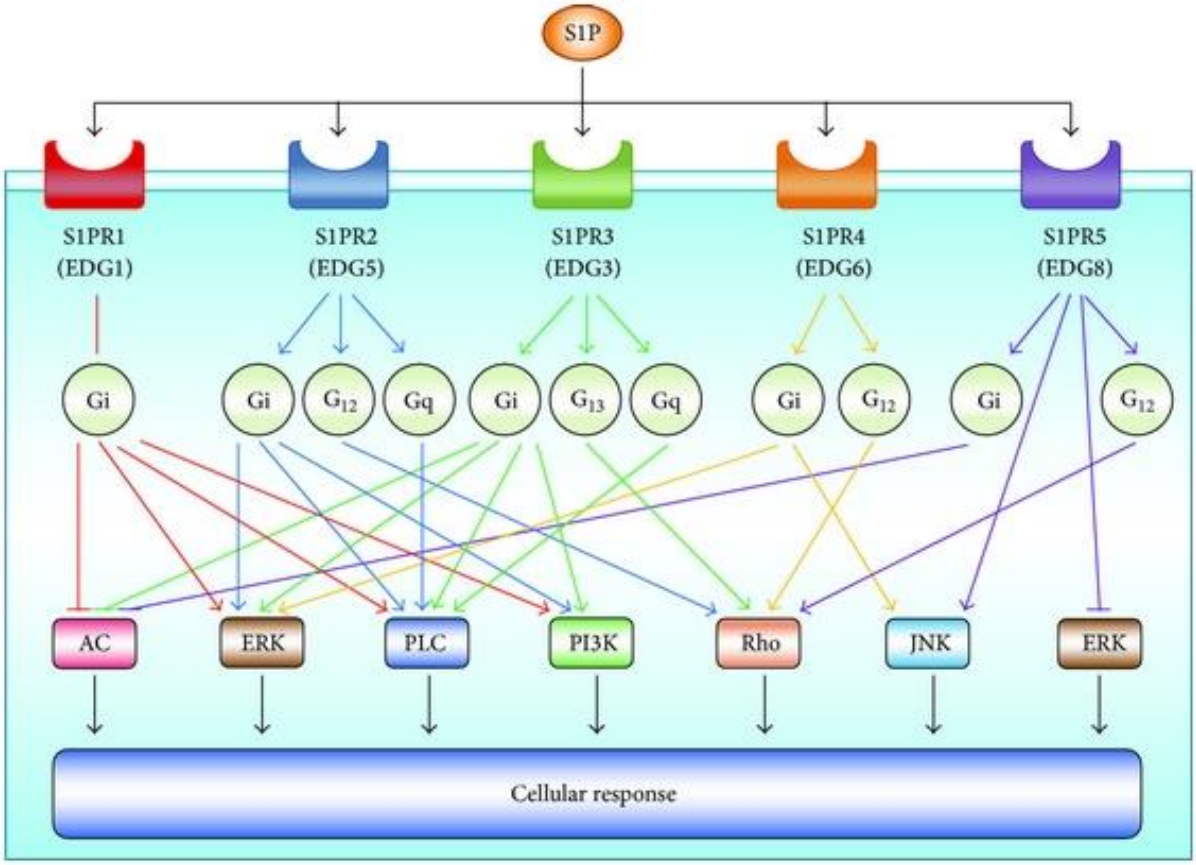

Figure 4: S1P and S1PR (1-5) Signaling Cascades – Adapted from Nagahashi, *et al.*, 2014

Each S1PR can couple with specific G proteins to regulate the activation or inhibition of a wide variety of downstream signaling processes, resulting in different cellular responses.

I.3.2 S1P and NPC Disease

As previously mentioned, S1P is a pro-proliferative molecule. Previous work has shown evidence that NPC mutant fibroblasts exhibit migratory defects [55], [56]. NPC cell models have also demonstrated that increased levels of sphingosine are accompanied by decreased levels of S1P which results in slowed endocytic trafficking, and retarded autophagosome maturation [18], [57], [58]. Additionally, previous work has exhibited that inhibiting SphK in normal wild type (WT) cells phenocopies the cholesterol storage defects seen in NPC cells, and that

overexpressing SphK1 activity reduces or corrects sphingosine accumulation, cholesterol trafficking, and autophagic defects observed in NPC [18]. These data suggest that there may be a deficiency in the role of SphK enzymes to synthesize S1P from sphingosine in NPC disease.

Significance

NPC is currently an incurable disorder that causes deficiencies in lysosomal proteins that are involved in lipid trafficking. S1PR signaling is known to be a driver in multiple diseases, and recent work has shown that the addition of nM concentrations of S1P or overexpression of SphK are able to restore some activation from the S1P receptors, and correct deficiencies observed in NPC mutant fibroblasts [59]. However, these methods of restoring cell function do not allow us to identify if any of the five receptors are potentially responsible for the pathology of NPC. Due to the relationship between NPC and S1P, we hypothesized that **the pathology of NPC is not solely due to the defective trafficking of cholesterol, but also to decreased S1P production and S1PR activation**. Owing to the wide range of downstream effects that the S1P/S1PR signaling system demonstrates, this study aimed to describe and assess the baseline levels of the S1P receptor's expression and activation in NPC disease, with the goal of identifying the specific S1PR(s) affected in NPC disease and to further explore the use of commercially available agonists/antagonists and their effects on deficiencies exhibited in NPC disease and possibly other related diseases.

Research Goals

Aim 1: To develop and optimize a panel of quantitative PCR assays to characterize the gene expression of the S1P receptors in *NPC1* mutant and knockout cells, and mouse tissue.

The goal of this aim was to develop and optimize a panel of qPCR assays to quantify the total mRNA present of each of the five S1P receptors in different cell and tissue samples, and to analyze and compare the amount of mRNA between NPC mutant samples and normal samples. Differences found in S1PR expression from qPCR analysis were then confirmed via western blot analysis.

Aim 2: To characterize the localization of the S1PR's in *NPC1* knockout cells and wild type cells through confocal microscopy.

The goal of this aim was to assess subcellular localization of S1P receptors. From the results of Aim 1, only S1PR1 and S1PR2 were subjected to immunostaining and fluorescence microscopy to determine their localization within WT and *NPC1* KO HeLa cells.

Aim 3: To examine the functionality of S1PR signaling systems in *NPC1* knockout and wild type cells.

The goal of this aim was to determine the biological consequences of the dysregulated expression of S1PR's in NPC disease. WT and *NPC1* KO cells were treated with commercially available S1PR1 and S1PR2 agonists and antagonists, and western blots were done to qualitatively and quantitatively analyze the presence, activation, and quantity of key downstream proteins in the S1PR1 and S1PR2 signaling cascade.

Chapter 1: Altered Gene Expression in S1PR1 and S1PR2 in *NPC1* Knockout Cells

1.1 Methods

1.1.1 Ethics Statement

Animal studies were conducted in conjunction with the VCU Massey Cancer Center Transgenic/Knockout Mouse Shared Resource Core Facility at Virginia Commonwealth University (VCU) in accordance with all institutional guidelines. All procedures were approved by the VCU Institutional Animal Care and Use Committee, which holds accreditation from the Association for Assessment and Accreditation of Laboratory Animal Care. Animals were given food and water *ad libitum* and kept on a 12-hour light/dark cycle for the duration of all experiments.

1.1.2 Cell Culture

The following control and *NPC1* mutant dermal fibroblasts used in this study were derived and obtained with consent from patients who were afflicted with NPC1 disease and were evaluated under a National Institute of Childhood Health and Human Development, NIH Review Board approved clinical protocol: *NPC5* (p. I1061T and p. R1186G), *NPC25* (fs-exon 20, c.2979dupA, and p. N701K), WTA (control). Wild type and *NPC1*$^{-/-}$ HeLa cells in which *NPC1* was knocked out (*NPC1* KO) using CRISPR/Cas9 editing were kindly provided by Dr. Wim Annaert (VIB Center for Brain and Disease Research, Leuven, Belgium) and have been described in previous work from this lab and others [60], [61]. All cells were cultured in 1X Dulbeco's Modified Eagle Medium (DMEM) with high glucose and pyruvate (ThermoFisher Scientific, #11995-065) with 10% Fetal Bovine Serum (FBS) and 1% penicillin/streptomycin.

1.1.3 Mice

The mice used in this study were initially obtained from The Jackson Laboratory and bred in house under a protocol approved by the VCU Institutional Animal Care and Use Program. *NPC1*$^{tm(I1061T)Dso}$ mutant mice (*NPC1*^{MUT} mice) possess *loxP* sites flanking exons 14-20 on the *NPC1* gene, as well as a missense mutation, I1061T, which is the most common found amongst humans afflicted with NPC1 disease [62].

1.1.4 Mouse Perfusion and Tissue Collection

Mice were anesthetized with isoflurane (NDS – 46066-755-04). Mice were then perfused with ice cold perfusate made of 1% heparin (ThermoFisher Scientific, #9041=08-1) in PBS. 11 mL of perfusate was pumped into the mice using a peristaltic pump at a rate of 6 mL/min. After perfusion, the mice's liver, brain, and cerebellum were carefully removed, snap frozen in liquid nitrogen (LN_2), and stored at -80°C until use.

1.1.5 RNA Extraction

To prepare cell samples for homogenization, cells in culture were trypsinized from their culture flask or plate and transferred into 15 mL conical tubes. The tubes were centrifuged for 5 minutes at 500 rpm to pellet cells before the supernatant was aspirated. To prepare tissue samples for homogenization, ~50mg of brain and liver tissues were weighed, flash frozen in dry ice, and crushed in a Multi-sample BioPulverizer (BioSpec, Bartlesville, OK, USA) that had been sterilized with ethanol and RNaseZAP (Sigma-Aldrich, #R2020), and pre-chilled in dry ice. Crushed tissue samples were scraped and transferred into a 15mL conical tube. All cell and tissue samples were homogenized by adding 1mL of Trizol Reagent (ThermoFisher Scientific,

#15596-018) into each conical tube and pipetted up and down until a homogeneous consistency was obtained. Cell and tissue homogenates were transferred into individual 1.5μL tubes and were stored in -80°C until used.

Homogenized samples were incubated for 10 minutes at room temperature to allow for complete dissociation. 1mL of homogenate was transferred into an Invitrogen Phasemaker tube (ThermoFisher Scientific, #A33248) with 0.2 mL of molecular biology grade chloroform. Samples were vortexed vigorously for 20 seconds then incubated at room temperature for 5 minutes before being centrifuged at 12,000 x g for 15 minutes at 2°C. Following the centrifugation, an upper aqueous phase is formed and separated from the lower red phenol phase by the Phasemaker gel. The upper aqueous phase was transferred to a fresh microcentrifuge tube, and RNA was precipitated out of the solution by adding 0.5mL of ice-cold isopropanol per 1mL of Trizol used for the initial homogenization. After the addition of isopropanol, samples were vortexed and incubated at room temperature for 10 minutes, then centrifuged at 12,000 x g for 10 minutes at 2°C. After this step, a translucent gel containing the RNA can be found pelleted at the bottom of the tubes. All the supernatant was removed carefully without disturbing the pellet and the RNA pellet was washed twice by adding 1mL of ice cold 75% ethanol, briefly vortexing, and centrifuging at 7,500 x g for 5 minutes at 2°C. All supernatant was removed, and RNA pellets were left to air dry inside of a sterilized biosafety cabinet for 10 minutes before being dissolved in 50μL of nuclease-free water. Samples were stored in -80°C until used.

1.1.6 DNase I Treatment and cDNA Synthesis

RNA samples were treated with DNase I using the Promega RQ1 DNase Kit (Promega, #M6101). RNA samples were quantified in a Biotek Epoch 2 Microplate Reader (Biotek, Winooski, VT, USA) and 2 μg of RNA were added into a tube containing 2 μL of Promega 10X DNase I reaction buffer and 2 μL DNase I. Nuclease free DEPC-treated water was added to each reaction to reach a final volume of 20 μL. Each reaction was then incubated at 37°C for 15 minutes. To deactivate the DNase I, 2 μL of 50 mM EDTA was added to each reaction and incubated at 65°C for 15 minutes.

All DNase I treated RNA were subjected to cDNA synthesis using the Applied Biosystems High-Capacity cDNA Reverse Transcription Kit (ThermoFisher Scientific, #4368814) and the provided random primers in a 20 μL reaction following the manufacturer's protocol. No-Template controls (distilled H_2O treated with DNase I) were also included during this step to screen for any contamination and to serve as a negative control.

1.1.7 Quantitative Real-Time PCR (qPCR)

All qPCRs were conducted using a Bio-Rad CFX Connect Real Time System (Bio-Rad, Hercules, CA, USA) and PowerUp™ SYBR Green Master Mix (ThermoFisher Scientific, #A25742). Primers that were designed to target the S1P Receptors, Sphingosine Kinase 1 and 2, and 18S rRNA sequences were utilized in the PCR in which the final concentration of each primer was 1 μM **(Table 2.1.1).** Each qPCR consisted of 2 μL of cDNA, 12 μL of PowerUp™ SYBR Green Master Mix, 1 μM of each primer, and nuclease free water to a final volume of 20 μL. Each reaction quantified one specific primer target in a sample, and each sample was analyzed in triplicate. All samples, along with a water control, were run in 96 well optical plates

(ThermoFisher Scientific, #N8010560) sealed with an adhesive optical film (ThermoFisher Scientific, #AB1170) with the following PCR program: 50°C for 2 minutes, 95°C for 2 minutes, followed by 40 cycles of a 15 second denature step at 95°C and a 2-minute annealing and extension step at 60°C.

After 40 cycles the PCR products were subject to a dissociation curve analysis. The first step of the dissociation curve analysis was at 95°C for 15 seconds, followed by a step at 60°C for 1 minute, then 70 cycles of heating for 15 seconds in 0.5°C increments from 50°C to 95°C with the fluorescence measured after each cycle.

1.1.8 Analysis of qPCR Data

To ensure specific amplicons were amplified in each reaction, a melt curve analysis was performed. Any reactions that yielded multiple melt curve peaks were subject to a gel electrophoresis to confirm whether one specific or multiple amplicons were produced. An average Ct value was calculated for each S1P receptor sample triplicate and was normalized to total 18S rRNA. The delta delta Ct ($2^{-\Delta\Delta Ct}$) method was used to calculate the genes fold change between cell types [63].

1.1.9 Statistical Analyses of qPCR Reactions

All qPCR data were analyzed using GraphPad Prism 9.0.2. The mean of the fold gene expression values calculated and the differences in the relative gene expression between normal and *NPC1* mutant cells were compared using multiple unpaired t-test. The *p*-value threshold for significance was set to $\alpha = 0.05$ and the *p*-value was corrected for multiple comparisons using the Holm-Šídák method.

1.1.10 Cell Harvesting, Homogenization, and Normalization

All cells were cultured as described above. Once the cells had grown to ~90% confluency inside the flasks, cells were counted using the Millipore Scepter cell counter (Sigma-Aldrich, St. Louis, MO, USA) and ~2.2 × 10^6 cells were seeded in sterile 10 cm petri dishes and starved in DMEM with no FBS overnight. After starving, plates were placed on ice and cells were washed twice with ice cold 1X PBS. Once washed, 500 μL of lysis buffer (HALT (ThermoFisher Scientific, #1861284) diluted 1:100 in 1X PBS) was added to each plate. Cells were manually scraped and transferred into 1.5 mL microcentrifuge tubes. Cells were then sonicated 3 times for 10 seconds each at 30% intensity and centrifuged at 5000 x g for 10 minutes at 4°C. After centrifuging, the resulting supernatant was transferred to a new tube and used for quantification.

Protein samples were quantified via the Bradford method [64]. A 1 mg/mL sample was made by dissolving 0.005 g of BSA in 5 mL of PBS, and serially diluted 1:10 six times to create working protein standards. 2 uL of each protein standard and unknown samples were loaded into a 96-well plate in triplicate with 200 μL of 1X Bio-Rad Protein Assay Dye solution (Bio-Rad, # 5000006). A standard curve was created in GraphPad Prism 9.0.2 using the protein standards and was deemed acceptable to use if R^2 value was at least 0.97. The protein concentration of each unknown sample was calculated using the standard curve. All samples were diluted to match the concentration of the least concentrated sample to ensure that equal amounts of protein were used for western blots.

1.1.11 Cell Treatment with Exogenous S1P

WT and *NPC1* KO HeLa cells were cultured as described in section 1.1.1. Once cells grew to ~95% confluency, cells were trypsinized, and ~2.2 × 10^6 cells were seeded into 10 cm

plates and starved overnight. After starving the cells, plates were placed on ice and washed twice with ice-cold 1X PBS. After washing, PBS was then aspirated from each plate and cells were treated with 100 nM of S1P dissolved in 1X PBS containing 4 mg/mL fatty-acid free BSA for 15 minutes each. After 15 minutes, S1P was aspirated from each plate and cells were washed once with ice cold PBS. Cells were then lysed with 500μL of Tris-NaCl-EDTA (TNE) lysis buffer (TNE Buffer (Quality Biological, #351302101), 20% glycerol, 0.1% Triton X) and were manually scraped into 1.5 mL microcentrifuge tubes. Cells were sonicated and quantified for western blot analysis as previously described.

1.1.12 Immunoblotting

Normalized protein samples were subjected to SDS-PAGE (10% - Tris-HCl) using the Bio-Rad Mini-PROTEAN Tetra System (Bio-Rad, Hercules, CA, USA). Samples were mixed with western blot loading buffer (250 mM Tris-HCl, 500 mM DTT, 10% SDS, 0.5% bromophenol blue, and 50% glycerol) and loaded into a 10% SDS-polyacrylamide gel along with the Bio-Rad Precision Plus Protein Dual Color Standard (Bio-Rad, #161-0394). Polyacrylamide gels were run at 150V until protein bands traveled about 95% down the gel (~45-50 min). After proteins were resolved, they were transferred onto a nitrocellulose membrane using the Invitrogen Power Blotter Station (ThermoFisher Scientific, Waltham, MA, USA) at 25V for 10 minutes. Once proteins were transferred, membranes were briefly rinsed with Tris-Buffered Saline (TBS) with 1% Tween-20 (ThermoFisher Scientific, #337-100) (TBS-T, pH ~7.4) and blocked with either 3% Bovine Serum Albumin (BSA) (Sigma-Aldrich, #A9647) or 5% Non-Fat Milk (Bio-Rad, #1706404) in TBS-T for at least 1 hour. Membranes were washed with 1X TBS-T for 10 minutes on a rocker three times before the membranes were incubated with the

appropriate primary antibody diluted 1:1000: S1PR1/EDG1 (ProteinTech, #55133), S1PR2 (ProteinTech, #21180). After primary antibody incubation, membranes were washed thoroughly with TBS-T for 10 minutes on a rocker three separate times. Membranes were then incubated on a rocker with a secondary horseradish-peroxidase conjugated anti-rabbit antibody (Cell Signaling Technology, #7074) diluted 1:1000 for 1 hour at room temperature. After secondary antibody incubation 3 more 10-minute washes were performed prior to incubation of the membrane with SuperSignal West Pico PLUS Chemiluminescent Substrate (ThermoFisher Scientific, #34577). Chemiluminescence was detected and imaged using a Bio-Rad ChemiDoc Imaging System. After imaging, membranes were stripped with 0.2 M NaOH for 10 minutes followed by three washes with 1X TBS-T for 10 minutes each. Stripped membranes were then similarly blotted for glyceraldehyde-3-phosphate dehydrogenase (GAPDH) (Cell Signaling Technology, #2118) diluted 1:5000 to serve as a loading control. Image J 1.53k software was used to quantify protein bands on western blots.

1.1.13 Statistical Analyses of Western Blot Reactions

Protein bands resulting from western blot reactions were quantified using Image J 1.53k software. GraphPad Prism 9.0.2 was used to compare the difference in total S1PR1 and S1PR2 proteins between WT and *NPC1* KO HeLa cells using an unpaired t-test.

Table 1: qPCR Primer Targets and Oligo Sequences

Target	Sequence 5' → 3'
Human S1PR1	Forward: CAG ACA AGC AAA ACA AAG TG
	Reverse: CAT CAA CAA AAG TGC CAA AG
Human S1PR2	Forward: ATA TAG AAT GGA GCA TGG GG
	Reverse: TTT TTG TGA AGT CCT TCT GG
Human S1PR3	Forward: AAG AGC CTA TGA AGG AGA AG
	Reverse: AGA ATC AAA GTG CTG TCT TG
Human S1PR4	Forward: CGC TTC TGT GTG ATT CTG
	Reverse: TGA TCG AAC TTC AAT GTT GC
Human S1PR5	Forward: AAA AGC ATT TCA GGA TGA GG
	Reverse: AGC GAA GTC CTC TAT ATC AC
Human SphK1	Forward: AAC TAC TTC TGG ATG GTC AG
	Reverse: TCC TGC AAG TAG ACA CTA AG
Human SphK2	Forward: CGT TTC CTT ATC AGG TTC AC
	Reverse: TCA GCT CTT AAG TAG GAC TTC
Mouse S1PR1	Forward: CAT GAG GTG AAA TGT GAG AG
	Reverse: AGT TGG TTG AAA TGG ATC AC
Mouse S1PR2	Forward: ATC CTG TCA TCT ATA CGT GG
	Reverse: CAG AAA TGT CGG TGA TGT AG
Mouse S1PR3	Forward: GAA CGA GAG CCT ATT TTC AAC
	Reverse: TCC TAG AGA CAG ATG GTT AC
Mouse S1PR4	Forward: CTT TGG TTC TAA TGT CTG GG
	Reverse: GAG GAT TAA TGG CTG AGT TG
Mouse S1PR5	Forward: GTT ACA GGA GAC TTT TGC AC
	Reverse: GTA GTG AAG GAC AAT AAC CTC
Human/Mouse 18S	Forward: CTC AAC ACG GGA AAC CTC AC
	Reverse: CGC TCC ACC AAC TAA GAA CG

1.2 Results

1.2.1 Selection of Primer Pairs for SYBR Green qPCR Assay to Detect For and Quantify S1P Receptor Expression

For the detection of the S1P receptors in WT and *NPC1* KO HeLa cells and human fibroblast cells, 27 different primer sequences were chosen that targeted the S1P receptors. Due to the unspecific nature and limitation of SYBR Green qPCR tests, different primers pairs were designed to flank different regions of the receptor's genes where the primer sequence and/or amplicons may span across an intron or be located at an exon-exon junction [65]. A qPCR reaction following the manufacturer's recommended protocol was run using each primer pair, and a melt curve analysis was done to determine the best primer pair for each target **(Figure 5)**. Primer pairs whose melt curves resulted in one peak indicated the presence of a single specific product and were selected to be used as the primer pairs to be used in this study **(Table 1)**.

1.2.2 Validation of qPCR Assay Efficiency

To analyze the gene expressions of our qPCRs, we first needed to determine whether our housekeeping gene (18S rRNA) and genes of interest (S1PR1-5) amplify with the same efficiency. The efficiency of a PCR is defined by the ratio of the number of target PCR products at the end of a cycle divided by the number of target PCR products at the start of the cycle. Theoretically a 100% efficient qPCR would double the number of target PCR products per cycle. In this study, the efficiency of the qPCR assay was determined by diluting HeLa WT cDNA 1:10 four times and running the samples using the optimized qPCR parameters and selected primer pairs in triplicate. The resulting Ct values were entered into GraphPad Prism 9.0.2 to create an efficiency curve. (**Figure 6)**. qPCR efficiency was determined using the formula Efficiency = -1

+ $10^{(-1/slope)}$ and efficiencies were determined to be acceptable if their PCR efficiency was between 90% - 110%. In addition to this calculation, the R^2 values of each curve were calculated and considered acceptable if their value was greater than or equal to 0.9. PCR efficiency was also visually compared by analyzing qPCR amplification plots (not shown).

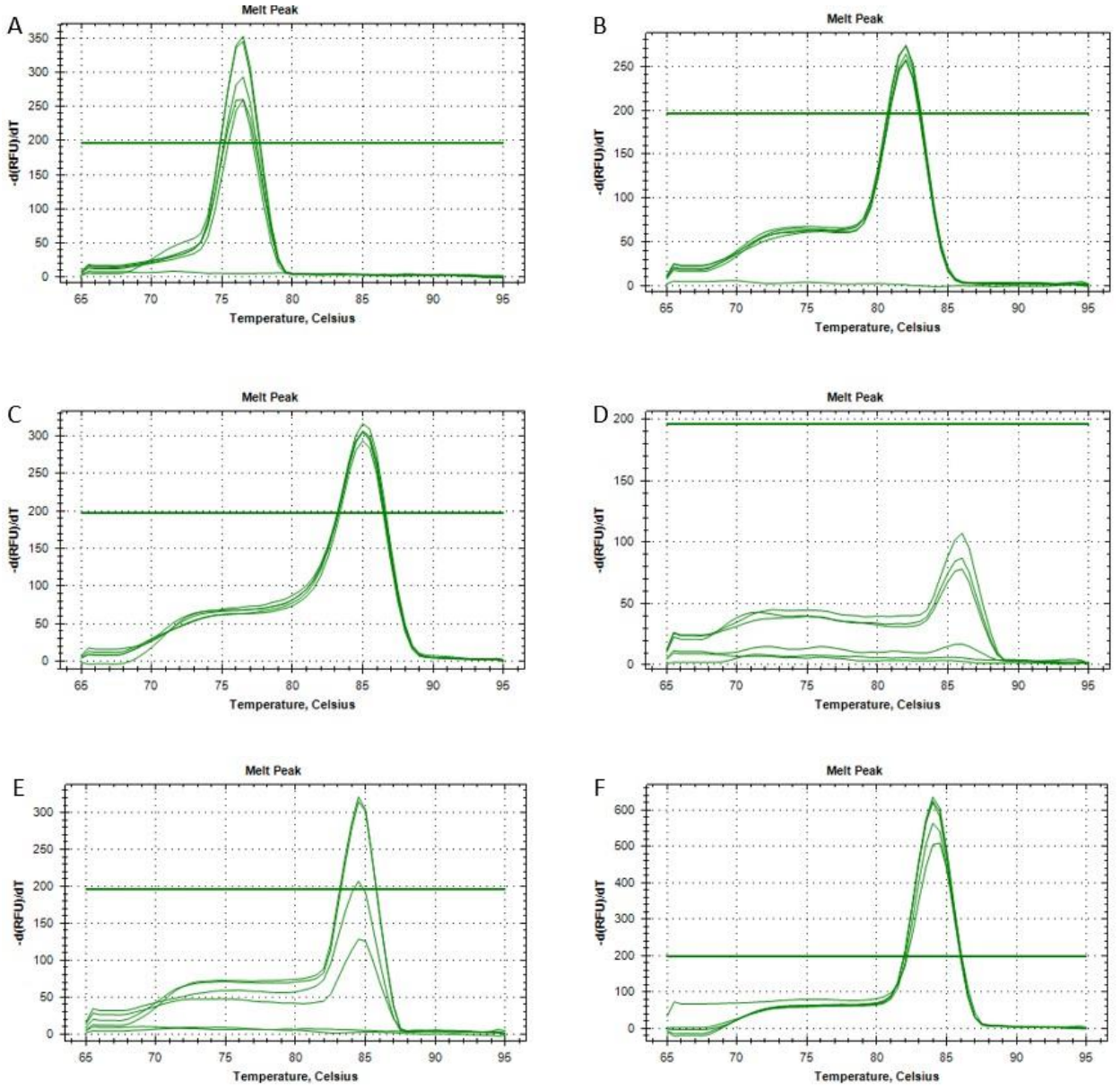

Figure 5: Melt Curve Peaks Obtained from SYBR Green qPCR Analysis

Primer pairs for S1PR1, S1PR2, S1PR3, S1PR5, and 18S rRNA show high sensitivity to their target genes. All melt curves were obtained from qPCRs using both WTA (n = 3) and *NPC5* (n = 3) human fibroblasts. The qPCR assays run are (A) S1PR1, (B) S1PR2, (C) S1PR3, (D) S1PR4, (E) S1PR5, (F) 18S rRNA. The temperature was plotted on the X-axis versus the negative first derivative of the reaction melt curve on the Y-axis. By plotting the negative first derivative of the reaction melt curve, it is easier to determine single peaks and pin-point the temperatures of dissociation.

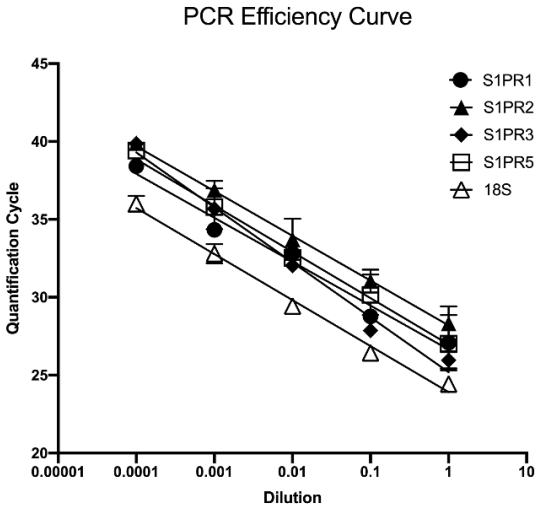

Gene Target	*Slope*	R^2	*PCR Efficiency*
S1PR1	-3.152 ± 0.181	0.95	107.6%
S1PR2	-3.096 ± 0.383	0.96	110.3%
S1PR3	-3.526 ± 0.376	0.97	92.1%
S1PR5	-2.971 ± 0.355	0.97	117.1%
18S rRNA	-3.120 ± 0.264	0.98	109.2%

Figure 6: qPCR Efficiency Validation for Human S1PR Panel

cDNA from HeLa WT cells was prepared for qPCR as described in 1.1.5-1.1.6. Total cDNA was diluted 1:10 four times and subject to the optimized qPCR assays for the S1PR's. Data are representative of three independent experiments of three biological replicates (n = 3) and are presented as best fit regression lines ± S.D., plotted on a semilog graph. Regression line slopes ± 95% Confidence Interval (CI), R^2 values and PCR efficiencies are reported. All PCR targets except for S1PR5 fell in the accepted 90% - 110% efficiency range.

1.2.3 S1P Receptors 1 and 2 Have Increased Expression in *NPC1* KO Cells and Mouse Brain and Liver Tissue

The relative expression of S1P receptors 1-5 in *NPC1* KO and mutant cells were compared to their expressions in WT cells. To compare the expression of the S1PR's relative to WT controls, cDNA from total RNA samples were used and run through the previously described optimized qPCR assays, and the fold change of each receptor was calculated using the delta delta Ct method and compared using a multiple unpaired t-test. Results from this experiment show that there is a significant increase of S1PR1 and S1PR2 in *NPC1* KO HeLa cells compared to WT HeLa cells. The average fold change for S1PR1, S1PR2, and S1PR5 in *NPC1* KO cells was 3.7, 3.3, and 2.8 times more than WT cells, respectively **(Figure 7)**. Mutant

human fibroblast cells were subjected to this panel of qPCRs and produced results that followed the trend observed in *NPC1* KO HeLa cells. Interestingly, the mutant fibroblasts also exhibited a decrease in S1PR5 mRNA, contradictory to the results seen in the HeLa cell data. This decrease could possibly be explained due to the cell type, as S1PR5 is more typically expressed in brain, spleen, and bone marrow tissue.

Initial results from the experiments conducted with mice livers and brains showed a significant increase in S1PR1 and S1PR2, similarly to the results of the *NPC1* KO HeLa cells **(Figure 7)**. It is important to note that the mouse primers were not fully optimized as were the human primers for S1PR1-5, and as an internal housekeeping gene, the 18S rRNA primer was designed to amplify a conserved region in both mice and humans.

1.2.4 Increased Expression of S1PR1 and S1PR2 in mRNA, but Similar Expression at the Protein Level

The total amount of S1PR1 and S1PR2 that is translated into their respective proteins was immunoblotted and total protein was calculated using ImageJ software. It was important that we calculated the total protein along with the total mRNA present because the observed increase in S1PR1, S1PR22 and S1PR5 mRNA do not necessarily correspond to increased protein production. WT and *NPC1* KO cells were treated with S1P and immunoblotted with S1PR1 and S1PR2 antibodies. As there is no commercially available primary monoclonal antibody for S1PR5, this target was not included for this analysis.

When treated with S1P there appears to be a decrease, although not a significant decrease, in the amount of S1PR1 and S1PR2 present in the cell **(Figure 8)**. This observed

decrease in S1PR1 and S1PR2, although contradicting the data found in the qPCR assays could suggest a possible interference in the translation of S1PR1 and S1PR2 into their protein products.

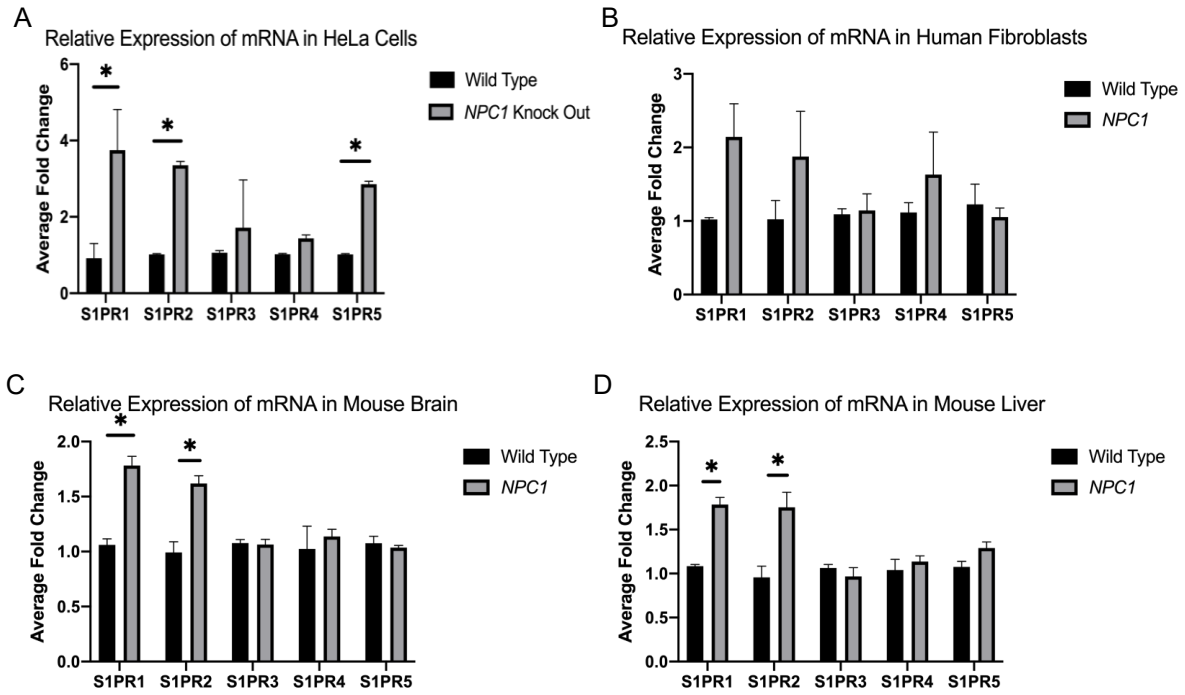

Figure 7: qPCR Relative Expression of S1PR1 – S1PR5 in HeLa Cells, Human Fibroblast Cells, and Mouse Brain and Liver Tissue

The mRNA of HeLa cells (A), human fibroblast (B), and mouse brain (C) and liver (D) tissue were subjected to the previously-described optimized assays for the S1PR's. The fold change of each receptor was determined by the $2^{-\Delta\Delta Ct}$ method, and normalized to WT control. HeLa and human fibroblast data are representative of three independent experiments that compared the S1PR's fold change from three biological replicates of *NPC1* KO and mutant cells (n = 3) to three biological replicates of WT HeLa cells and WTA human fibroblast cells (n = 3). Mouse brain and liver tissue data are representative of three independent experiments that compared the S1PR's fold change from three biological replicates of $NPC1^{MUT}$ mice (n = 3) and to WT mice (n = 3). Data is presented as the mean fold change value ± S.D. All p-values were determined by a multiple unpaired t-test. The p-value threshold for significance was set to $\alpha = 0.05$ and p-values were corrected for multiple comparisons using the Holm-Šídák method. *, $p < 0.05$ compared to WT. The relative expression of S1PR1 was significantly higher ($p = 0.01$) in *NPC1* KO HeLa cells compared to WT HeLa cells. There was also a significant increase in S1PR2 and S1PR5 ($p < 0.001$). WT and *NPC1* mutant fibroblasts followed a similar trend as the HeLa cells, with the exception of S1PR5. Mouse brain and liver mRNA exhibited a similar expression pattern to the HeLa cells with significant increases in S1PR1 and S1PR2 ($p < 0.001$).

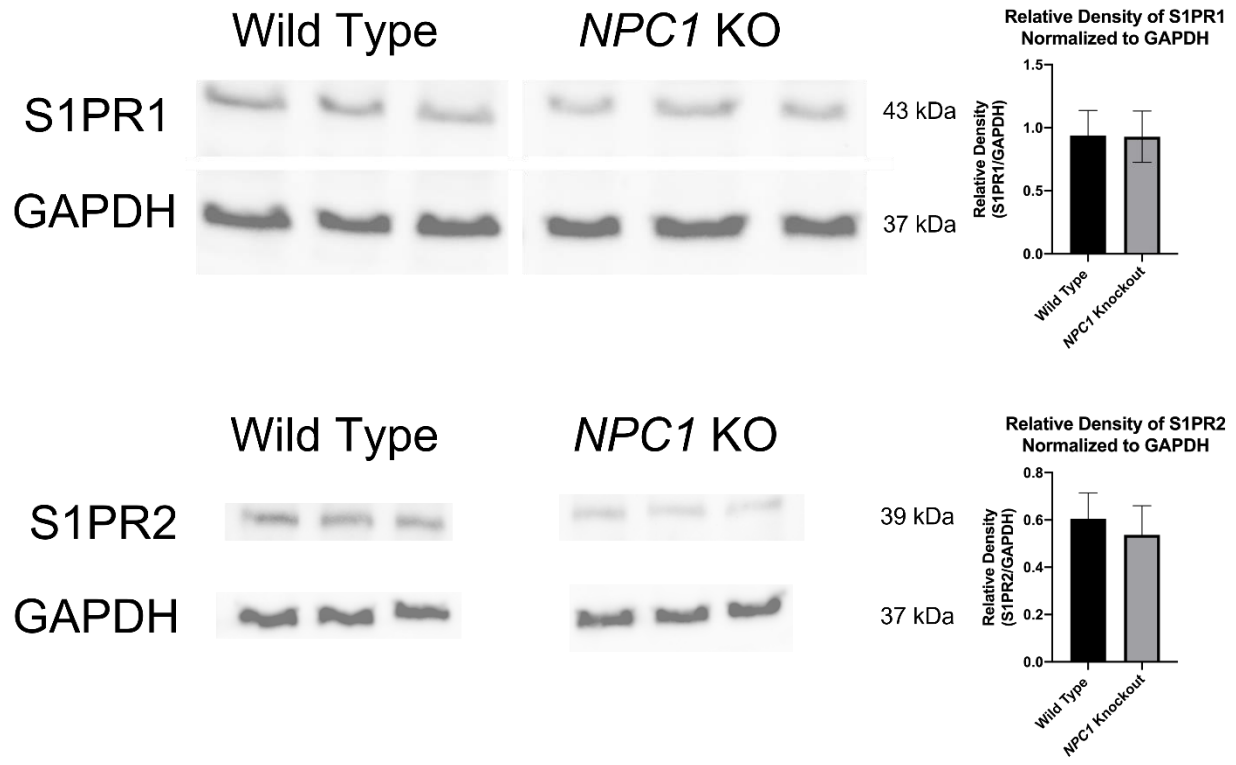

Figure 8: Western Blots of S1PR1 and S1PR2 treated with S1P

WT and *NPC1* KO HeLa cells were treated with 100 nM of S1P for 15 minutes, and cell lysate proteins were immunoblotted with specific antibodies that targeted S1PR1 and S1PR2. Blots were then stripped and re-blotted with GAPDH specific antibodies to show equal transfer and loading of samples. Blots are representative of three independent experiments of technical triplicates of HeLa WT (n = 1) and *NPC1* KO (n = 1) cells. The optical density of each band was quantified using Image J 1.53k software and the optical density (OD) of S1PR1 and S1PR2 bands were normalized to GAPDH. Relative OD of S1PR1 and S1PR2 in WT cells were compared to the relative OD of S1PR1 and S1PR2 in *NPC1* KO cells using an unpaired t-test. Data are means ± S.D. of the presented blots. No significant changes in S1PR1 and S1PR2 proteins were observed in *NPC1* KO HeLa cells.

1.3 Discussion

S1P is a potent bioactive molecule that is a positive regulator of cell proliferation, motility, and survival [16], [20]. Defects in NPC mutant cell activity can be attributed to the apparent lack of S1P such as evidence of fibroblast migration, slowed endocytic trafficking, and slowed autophagosome maturation [18], [55]–[58]. Owing to our deeper understanding of sphingolipids and the apparent role that deficient S1P has on the pathology of NPC, we hypothesized that the pathology of NPC is not solely due to deficient cholesterol trafficking, but also attributed to the lack of S1P production and activation of the S1PR's. This study aimed to address our hypothesis by focusing on elucidating the S1P/S1PR interactions that may be associated with the difficulties observed in NPC.

By creating multiple primers that flanked different regions of our genes of interest, we were able to optimize a qPCR panel that was able to consistently amplify 18S rRNA, S1PR1, S1PR2, and S1PR3, with similar amplification efficiencies **(Figures 5 and 6)**. In HeLa cells, our qPCR assay suggests that compared to WT HeLa cells, *NPC1* KO HeLa cells exhibit a significant increase of S1PR1, S1PR2, and S1PR5 mRNA expression. A similar trend toward an increase was observed for S1PR1 and S1PR2 mRNA expression in WT and mutant human fibroblast cells. These findings indicate a possible upregulation of S1PR1 and S1PR2, most likely in response to the decreased activation of these receptors due to the lack of S1P **(Figure 7)**. Interestingly and contradictory to our HeLa cell mRNA expression data, *NPC1* mutant fibroblast cells exhibited a decrease in S1PR5 mRNA expression. This observation is possibly due to the differences in cell types, as S1PR5 mRNA is not commonly expressed in connective tissue but is expressed in cervical tissue [66]

In addition to human cell lines, mRNA from the brain and liver tissue of male and female *NPC1*^{MUT} mice were also analyzed. Similar to our human cell line assays, multiple primer pairs that flanked different regions of our genes of interest were tested and an optimized panel of primer pairs were chosen based on their ability to produce a strong and singular signal from a melt curve analysis. However, due to time restraints from the availability of mouse tissue, the amplification efficiencies of these assays were not assessed. Preliminary data from our *NPC1*^{MUT} mouse tissue exhibited a trend toward increase in S1PR1 and S1PR2; however, these results were not significant as seen with our human fibroblast data. There was no apparent difference in mRNA expression between male and female mice.

Due to the consistent increase observed in S1PR1 and S1PR2 across cell and tissue analyses, these proteins were used as targets for a western blot analysis. Although S1PR5 was also observed to be significantly increased in *NPC1* KO HeLa cells, this target was not analyzed due to the lack of a quality commercially available antibody to target S1PR5. Immunoblots were performed using HeLa WT and *NPC1* KO cells. In contrast to our qPCR data, initial results from immunoblotting S1PR1 and S1PR2 indicate that there is no difference in the total S1PR1 or S1PR2 in *NPC1* KO HeLa cells. Although the contradicting qPCR and western blot data can be an indication of a problem in the translation of the S1PR's or possibly the trafficking of the S1PR's to the plasma membrane. However, it is most likely that the inconsistencies between western blot and qPCR data can be attributed to human error.

Future Directions

In the future, this study should more accurately optimize both the human cell line and mouse tissue qPCR assays to determine that the PCR efficiencies not only match but are

amplifying our genes of interest as close to 2-fold for every PCR cycle as possible. Given the nature of the $2^{-\Delta\Delta Ct}$ equation used to calculate the genes fold change between cell types, the closer our qPCR reactions are to 100% efficiency, the more accurate the calculation will be [63]. By transforming our genes of interest into plasmids in *E. coli* bacteria, successfully transformed *E. coli* can be selected and plasmids can be extracted and counted to create sample standards used to more accurately and precisely calculate PCR efficiency.

In addition to more accurate PCR efficiency readings, western blot analyses for S1PR1 and S1PR2 should be done to confirm the findings from the HeLa cell experiments. Although the decrease of S1PR1 and S1PR2 exhibited in HeLa cells is not statistically significant, it would be of interest to see if a similar trend is also found in our human fibroblast cells and mouse tissue.

Chapter 2: Cellular Localization of S1PR1 and S1PR2 Proteins

2.1 Methods

2.1.1 Immunostaining and Confocal Microscopy

WT and *NPC1* KO HeLa cells from culture were trypsinized and counted using the Millipore Scepter cell counter. 10,000 cells were seeded in each well of a Cellvis 24 Well Glass Bottom Plate and starved with DMEM containing no FBS overnight. Starvation medium was aspirated, and wells were washed twice with phosphate buffered saline (PBS). Cells were fixed in their wells with 3.7% paraformaldehyde (ThermoFisher Scientific, #AA47377-9L) in PBS for 15 minutes, then washed three times with 10mM Glycine (ThermoFisher Scientific, #BP381-1) in PBS. Dependent on the experimental design, some cells were permeabilized in order to stain internal epitopes with 0.5% Triton X-100 (Sigma-Aldrich, #T8787) diluted in PBS for 3 minutes followed by 2 more washes with 10mM Glycine/PBS. Cells were incubated for an hour with the appropriate antibodies diluted 1:1000: S1PR1/EDG1 (ProteinTech, #55133) or S1PR2 (ProteinTech, #21180). Following primary antibody incubation, cells were washed 3 times with 10mM Glycine/PBS and were incubated with Alexa Fluor Plus 488 conjugated anti-rabbit secondary antibody/probe (ThermoFisher Scientific, #A32731) diluted 1:1000 for 1 hour. The probe was aspirated, and all cells were washed with DAPI fluorescent stain (Sigma-Aldrich, #D9542) diluted 1:5000 for 10 minutes, followed by 2 more washes with 10mM Glycine/PBS for 10 minutes each. 4mL of 10mM Glycine/PBS were added into each well to preserve the cells, and cells were visualized under a Keyence BZ-X Series fluorescence microscope (Keyence, Osaka, Japan).

2.2 Results

2.2.1 Localization of S1PR1 and S1PR2

The increased mRNA expression of S1PR1, S1PR2, and S1PR5 that was observed in our *NPC1* KO HeLa cells and in our *NPC1*^{MUT} mice in the previous aim may suggest that more receptors are being produced, however successful trafficking of the receptors to the plasma membrane needs to occur for any action to take place. To investigate this, the subcellular localization of S1PR1 and S1PR2 was determined through confocal microscopy using antibodies specific for each of the receptors. Note that due to the lack of a reliable antibody that is specific to S1PR5, these receptors were not immunostained in this experiment.

Cells were fixed in glass bottom wells and stained with the appropriate antibodies for S1PR1 and S1PR2. Initial results show that *NPC1* KO cells have a decrease in transmembrane S1PR2 in comparison to the WT, whereas there was a similar presence of transmembrane S1PR1 in both *NPC1* KO and WT HeLa cells **(Figure 9)**. The increased transcription of S1PR2 observed in the previous experiment and the observed decrease of transmembrane S1PR2 can indicate that there is a deficiency of S1PR2 being trafficked to the plasma membrane.

In an attempt to further investigate the lack of transmembrane S1PR2, WT and *NPC1* KO HeLa cells were permeabilized to attempt to stain internal epitopes of S1PR1 and S1PR2. These results, however, were inconclusive as the permeabilization of the cells was apparently unsuccessful.

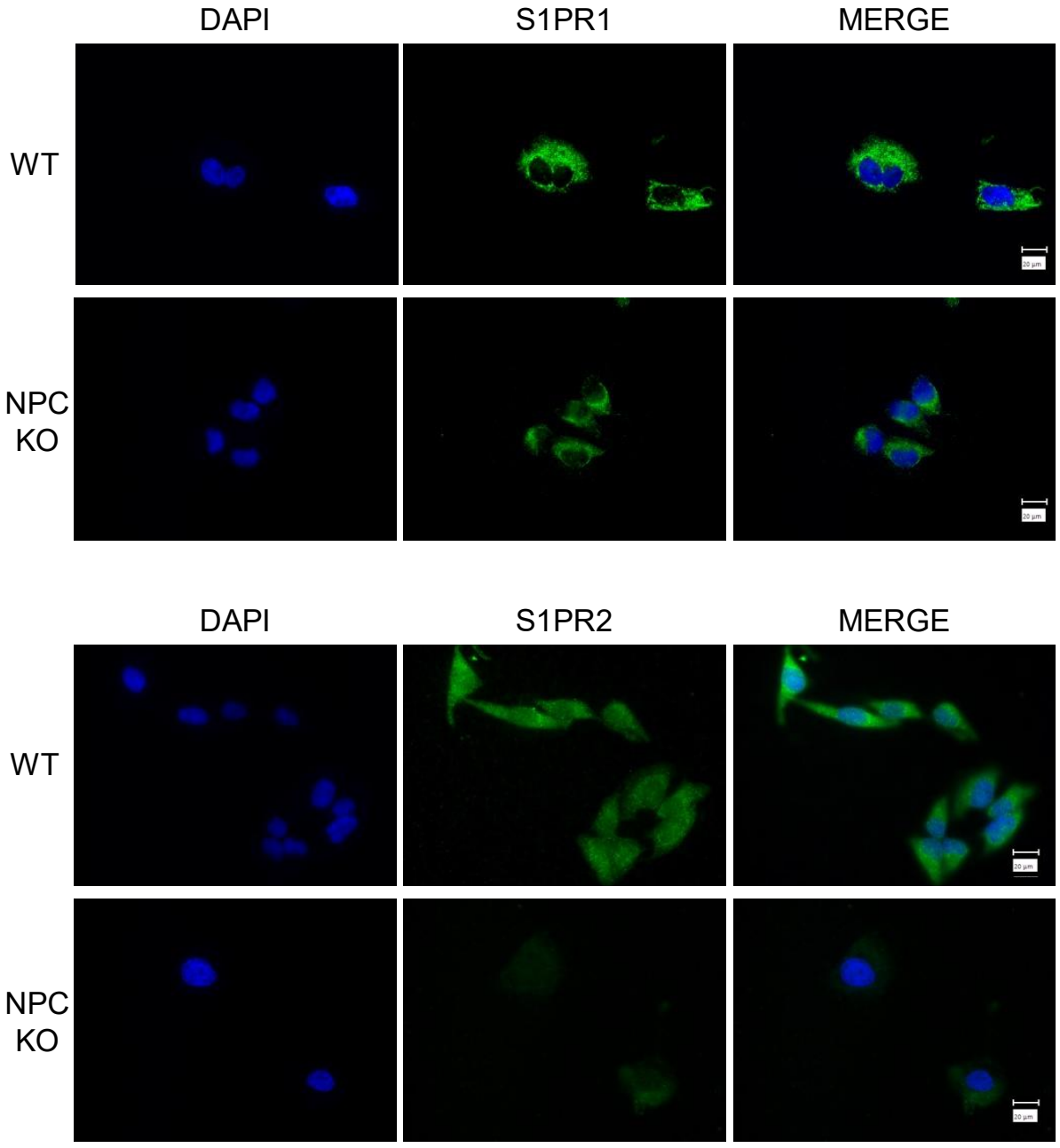

Figure 9: Non-Permeabilized Fluorescence Microscopy Images of S1PR1 and S1PR2 in HeLa Wild Type and *NPC1* KO Cells

WT and *NPC1* KO HeLa cells were immunostained with DAPI (Blue) as a nuclear stain and with antibodies that specifically bind to either S1PR1 or S1PR2 followed by the ThermoFisher Alexa Fluor 2º conjugated antibody (Green). Cells were then analyzed under a fluorescent microscope to determine subcellular localization of the receptors. *Scale bars,* 20 µm.

2.3 Discussion

The inside-out signaling S1P requires the transport of S1P outside of the cell to activate one of the five S1PR's on the plasma membrane. As shown in the previous aim of this study there was no difference in the total amount of S1PR1 and S1PR2 in HeLa *NPC1* KO cells which contradicted the initial qPCR results displaying an increase in mRNA present for those two receptors. These results indicated a possibility that there may also be a problem with either the translation of the S1PRs from their mRNA to their respective protein products, or a problem regarding the transport of the receptors to the plasma membrane. To address these questions, an attempt to determine the localization of S1PR1 and S1PR2 in WT and *NPC1* KO HeLa cells was done by immunostaining cells with DAPI and either S1PR1 or S1PR2 primary antibodies and observing WT and *NPC1* KO cells using fluorescence microscopy.

Visually, cells that were immunostained showed similar localization and intensity of S1PR1 at the plasma membrane of both WT and *NPC1* KO HeLa cells. In contrast, images taken of S1PR2 visually show a decrease in intensity of S1PR2 around the plasma membrane of *NPC1* KO cells compared to WT HeLa cells. The decrease in intensity may indicate that less receptors are being transported to the cell membrane.

To address whether there is a lack of transport of S1PR2 to the plasma membrane, an attempt to stain the internal epitopes of S1PR1 and S1PR2 was done by permeabilizing WT and *NPC1* KO cells with 0.5% Triton X-100. Unfortunately, the permeabilization of the HeLa cells was unsuccessful and we could not determine whether S1PR2 was accumulating inside the cell.

Future Experiments

The largest pitfall of this experiment was the failure to successfully permeate the cell membrane to stain any internal S1PR1 or S1PR2 epitopes that may be present. This should be the first point to address in this experiment to answer the question whether there may be any issues with transport or translation of these receptors in *NPC1* KO cells. Access to a confocal microscope may also clarify areas of DAPI and S1PR stain overlap in our fluorescent microscope images to determine whether the overlap is due to poor staining, or if the overlap is due to the transmembrane S1PR's being stained above the nucleus. Unfortunately, however, further investigation of the other receptors by fluorescence microscopy is highly limited due to the lack of quality antibodies that target any of the other S1P receptors.

Chapter 3: Functionality of S1PR1 and S1PR2 Signaling Cascades in HeLa Wild Type and *NPC1* Knockout Cells

3.1 Methods

3.1.1 Cell Treatment with S1PR Agonists and Antagonists

WT and *NPC1*$^{-/-}$ HeLa cells were cultured, starved, and washed as previously described. After washing plates with ice cold 1X PBS, cells were treated for 10 minutes with 10 μM of S1PR1 or S1PR2 Agonist or Antagonist drug **(Table 2)**. After drug treatment, cells were washed once more with ice cold 1X PBS and lysed with TNE lysis buffer. Cells were manually scraped into 1.5mL microcentrifuge tubes, sonicated, and quantified for western blot analysis as previously described.

Table 2: S1PR1 and S1PR2 Agonist and Antagonist Drugs

Target	***Agonist Drug***	***Antagonist Drug***
S1PR1	SEW 2871	W123
S1PR2	CYM 5520	JTE-013

3.1.2 Immunoblotting

Western blot analysis was performed as described in section 1.1.12. The following primary antibodies were diluted 1:1000 and used in this panel to assess signaling cascade functionality in HeLa *NPC1* KO cells: Akt (Cell Signaling Technology, Cat. #4060), Phospho-Akt (Cell Signaling Technology, #4691), p44/42 MAPK (Cell Signaling Technology, #4695), Phospho-p44/42 MAPK (Cell Signaling Technology, Cat. #4377), GAPDH (Cell Signaling Technology, #2118).

3.1.3 Statistical Analyses of Western Blot Reactions

Protein bands resulting from western blot reactions were quantified using Image J 1.53k software, and the relative density of each downstream target was normalized to GAPDH. GraphPad Prism 9.0.2 was used to compare the relative densities of each downstream target in *NPC1* KO cells to WT cells using multiple t-tests where the *p*-value threshold for significance was set to $\alpha = 0.05$ and *p*-values were corrected for multiple comparisons using the Holm-Šídák method.

3.2 Results

3.2.1 S1PR2 Decreased Activation of AKT Pathway With S1PR2 Agonist

To investigate the functionality of the S1PR1 and S1PR2 signaling cascades, WT and *NPC1* KO HeLa cells were grown and treated with either SEW 2871 (S1PR1 agonist), CYM 5520 (S1PR2 agonist), W123 (S1PR1 antagonist), or JTE-013 (S1PR2 antagonist) (**Table 2)**. Western blots of each cell treatment were performed targeting two key downstream proteins, including their phosphorylated forms, with the goal of elucidating their downstream activation in NPC disease and identifying drugs of interest that can be further explored to treat NPC disease.

Initial results of this experiment show that the activation of AKT is significantly decreased in *NPC1 KO* cells in response to CYM 5520 (S1PR2 agonist). Further, when *NPC1* KO cells are introduced to JTE-013 (S1PR2 antagonist), activation of the AKT is restored.

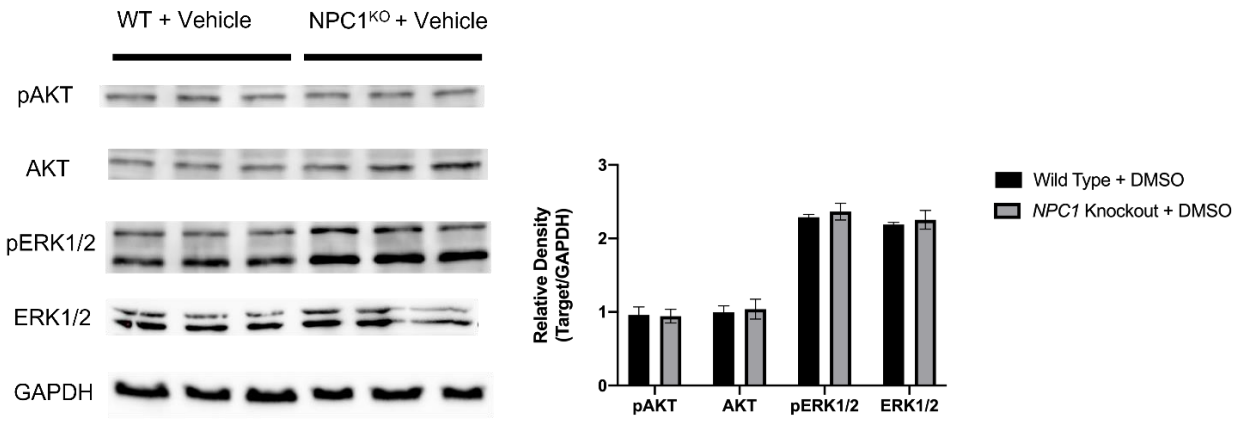

Figure 10: Western Blot of pAKT, AKT, pERK1/2, and ERK in WT and *NPC1* KO Cells Treated with DMSO

WT and *NPC1* KO HeLa cells were treated with a DMSO vehicle for 10 minutes, and cell lysate proteins were immunoblotted with specific antibodies that targetted the following proteins: pAKT, AKT, pERK1/2, and ERK1/2. Blots were then stripped and re-blotted with GAPDH specific antibodies to show equal loading of samples. Images and data are representative of three independent experiments, each with three biological replicates ($n = 3$). The OD of each band was quantified using Image J 1.53k software and the relative density of each target was normalized to GAPDH. The relative OD of each target in WT cells were compared to their respective counterparts in *NPC1* KO cells using multiple unpaired t-tests where the p-value threshold for significance was set to $\alpha = 0.05$ and corrected for multiple comparisons using the Holm-Šídák method. Data shown are means ± S.D. of the presented blot. No noticeable nor statistical increases or decreases were observed in these cells.

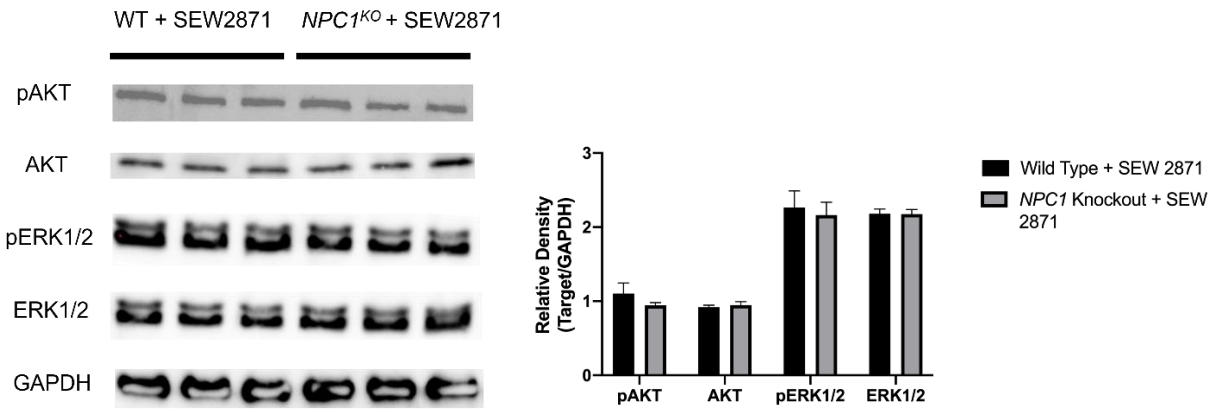

Figure 11: Western Blot of pAKT, AKT, pERK1/2, and ERK in WT and *NPC1* KO Cells Treated with S1PR1 Agonist SEW-2871

WT and *NPC1* KO HeLa cells were treated with 10 μM of S1PR1 agonist SEW 2871 for 10 minutes, and cell lysate proteins were immunoblotted with specific antibodies that targetted the following proteins: pAKT, AKT, pERK1/2, and ERK1/2. Blots were then stripped and re-blotted with GAPDH specific antibodies to show equal loading of samples. Images and data are representative of three independent experiments, each with three biological replicates (n = 3). The OD of each band was quantified using Image J 1.53k software and the relative density of each target was normalized to GAPDH. The relative OD of each target in WT cells were compared to their respective counterparts in *NPC1* KO cells using multiple unpaired t-tests where the p-value threshold for significance was set to $\alpha = 0.05$ and corrected for multiple comparisons using the Holm-Šídák method. Data shown are means ± S.D. of the presented blot. No noticeable nor statistical increases or decreases were observed in these cells.

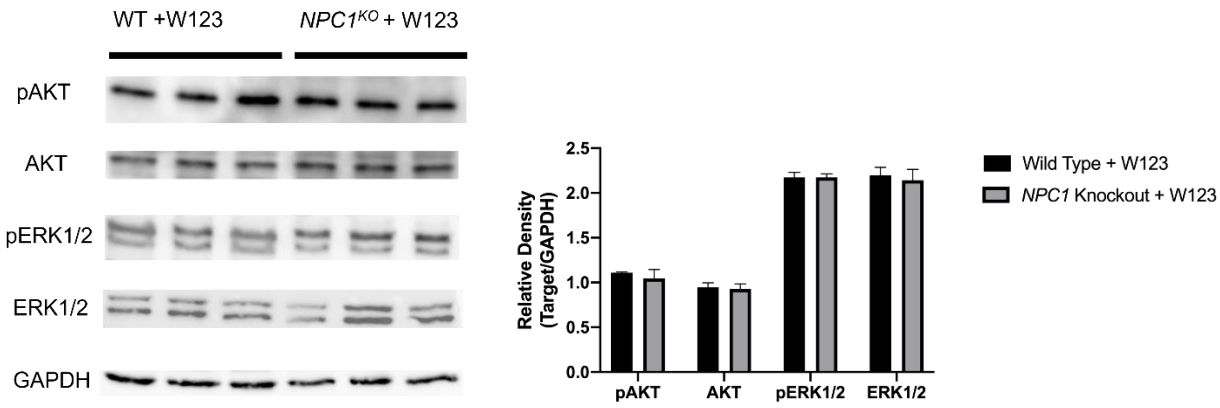

Figure 12: Western Blot of pAKT, AKT, pERK1/2, and ERK in WT and *NPC1* KO Cells Treated with S1PR1 Antagonist W123

WT and *NPC1* KO HeLa cells were treated with 10 μM of S1PR1 antagonist W123 for 10 minutes, and cell lysate proteins were immunoblotted with specific antibodies that targetted the following proteins: pAKT, AKT, pERK1/2, and ERK1/2. Blots were then stripped and re-blotted with GAPDH specific antibodies to show equal loading of samples. Images and data are representative of three independent experiments, each with three biological replicates ($n = 3$). The OD of each band was quantified using Image J 1.53k software and the relative density of each target was normalized to GAPDH. The relative OD of each target in WT cells were compared to their respective counterparts in *NPC1* KO cells using multiple unpaired t-tests where the p-value threshold for significance was set to $\alpha = 0.05$ and corrected for multiple comparisons using the Holm-Šídák method. Data shown are means ± S.D. of the presented blot. No noticeable nor statistical increases or decreases were observed in these cells.

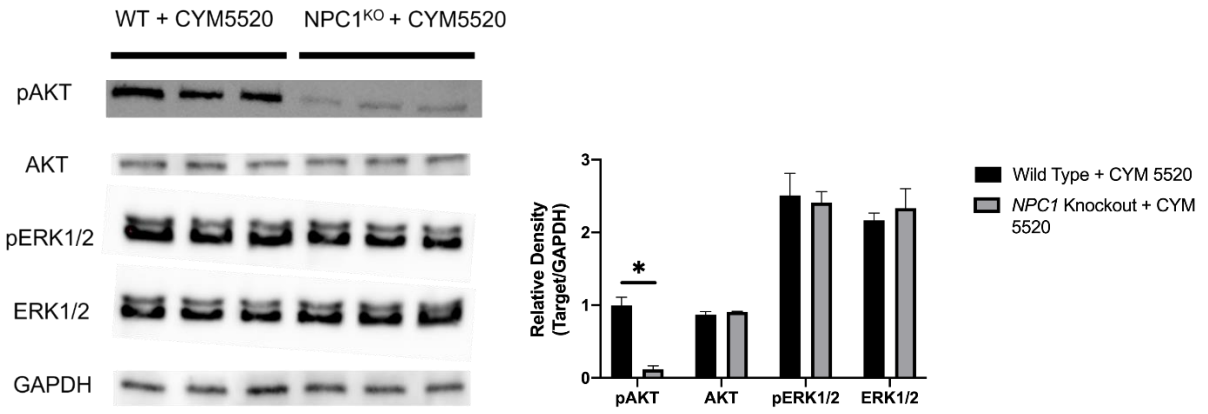

Figure 13: Western Blot of pAKT, AKT, pERK1/2, and ERK in WT and *NPC1* KO Cells Treated with S1PR2 Agonist CYM-5520

WT and *NPC1* KO HeLa cells were treated with 10 μM of S1PR2 agonist CYM 5520 for 10 minutes, and cell lysate proteins were immunoblotted with specific antibodies that targetted the following proteins: pAKT, AKT, pERK1/2, and ERK1/2. Blots were then stripped and re-blotted with GAPDH specific antibodies to show equal loading of samples. Images and data are representative of three independent experiments, each with three biological replicates ($n = 3$). The OD of each band was quantified using Image J 1.53k software and the relative density of each target was normalized to GAPDH. The relative OD of each target in WT cells were compared to their respective counterparts in *NPC1* KO cells using multiple unpaired t-tests where the p-value threshold for significance was set to $\alpha = 0.05$ and corrected for multiple comparisons using the Holm-Šídák method. Data shown are means ± S.D. of the presented blot. *, $p < 0.05$ compared with WT. A significant decrease ($p = 0.009$) of pAKT was observed in *NPC1* KO cells compared to WT.

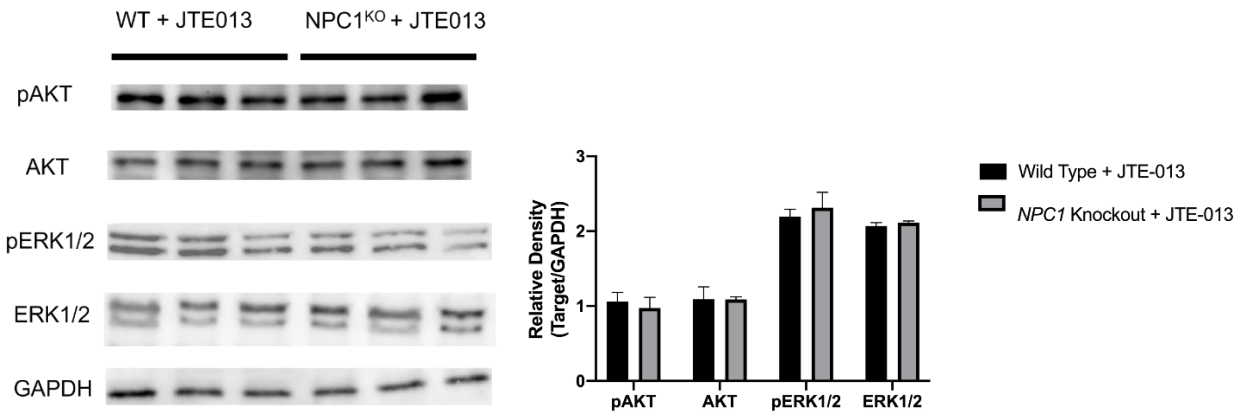

Figure 14: Western Blot of pAKT, AKT, pERK1/2, and ERK in WT and *NPC1* KO Cells Treated with S1PR2 Antagonist JTE-013

WT and *NPC1* KO HeLa cells were treated with 10 μM of S1PR2 agonist CYM 5520 for 10 minutes, and cell lysate proteins were immunoblotted with specific antibodies that targetted the following proteins: pAKT, AKT, pERK1/2, and ERK1/2. Blots were then stripped and re-blotted with GAPDH specific antibodies to show equal loading of samples. Images and data are representative of three independent experiments, each with three biological replicates ($n = 3$). The OD of each band was quantified using Image J 1.53k software and the relative density of each target was normalized to GAPDH. The relative OD of each target in WT cells were compared to their respective counterparts in *NPC1* KO cells using multiple unpaired t-tests where the *p*-value threshold for significance was set to $\alpha = 0.05$ and corrected for multiple comparisons using the Holm-Šídák method. Data shown are means ± S.D. of the presented blot. A restoration of pAKT was observed when *NPC1* KO cells were treated with the S1PR2 antagonist drug.

3.3 Discussion

The use of GPCR's as a drug target has recently been increasing in popularity because of the wide variety of human processes that they can regulate. The goal of the current experiment was to determine the functionality of some key downstream proteins in NPC disease and observe how their activation may differ in the presence of either S1PR1 or S1PR2 agonist or antagonist drugs. The two downstream targets that were chosen for this experiment, along with their activated states, were the phosphoinositide-3-kinase (P13K or AKT) pathway and the mitogen-activated protein kinase (MAPK or ERK) signaling pathway because of their importance and abundance in the cell, and their common activation and association in response to both S1PR1 and S1PR2 **(Figure 4)**.

Across the panel, the only significant difference that was observed was a decrease (p = 0.009) in the activation of the AKT pathway when *NPC1* KO cells are treated with CYM-5520 an agonist of S1PR2 **(Figure 13)**. Conversely, the decreased activation of the AKT pathway was observed to be restored when NPC1 KO cells were treated with the S1PR2 antagonist drug JTE-013 **(Figure 14)**. S1PR2 plays a pivotal role in many biological processes including survival, proliferation, and cellular metabolic regulation. Similarly to our observations, another study has also observed that decreased activation of the AKT pathway by S1PR2 can be restored by the blockage of S1PR2 using the antagonist drug JTE-013 [67]. These observations suggest that there may be a deficiency in the S1PR2 signaling cascade in NPC disease, and that a dysfunctional S1PR2 may play a key role in the pathology of NPC disease. Due to this, S1PR2 could be considered a viable drug target for the treatment of NPC disease.

Future Experiments

Although this study shows the restoration of pAKT when treated with JTE-013, further studies are needed to elucidate the molecular intricacies of S1PR2's regulation of the AKT pathway. Additionally, since S1PR2 is generally expressed in all cell types, it would be of interest would be to investigate whether the decreased pAKT and restoration by S1PR2 agonist and antagonist interactions are present in other human cells lines, as well as in human or mouse tissue. Furthermore, the effect of JTE-013 on S1P treated cells may also uncover some details on the drug's capability to restore pAKT when competition for the receptor is introduced.

Literature Cited:

[1] E. D. Carstea *et al.*, "Niemann-Pick C1 Disease Gene: Homology to Mediators of Cholesterol Homeostasis," *Science*, vol. 277, no. 5323, pp. 228–231, Jul. 1997, doi: 10.1126/science.277.5323.228.

[2] H. J. Kwon *et al.*, "Structure of N-terminal domain of NPC1 reveals distinct subdomains for binding and transfer of cholesterol," *Cell*, vol. 137, no. 7, pp. 1213–1224, Jun. 2009, doi: 10.1016/j.cell.2009.03.049.

[3] M. L. Wang *et al.*, "Identification of surface residues on Niemann-Pick C2 essential for hydrophobic handoff of cholesterol to NPC1 in lysosomes," *Cell Metab.*, vol. 12, no. 2, pp. 166–173, Aug. 2010, doi: 10.1016/j.cmet.2010.05.016.

[4] X. Xie, M. S. Brown, J. M. Shelton, J. A. Richardson, J. L. Goldstein, and G. Liang, "Amino acid substitution in NPC1 that abolishes cholesterol binding reproduces phenotype of complete NPC1 deficiency in mice," *Proc. Natl. Acad. Sci. U. S. A.*, vol. 108, no. 37, pp. 15330–15335, Sep. 2011, doi: 10.1073/pnas.1112751108.

[5] S. R. Pfeffer, "NPC intracellular cholesterol transporter 1 (NPC1)-mediated cholesterol export from lysosomes," *J. Biol. Chem.*, vol. 294, no. 5, pp. 1706–1709, Feb. 2019, doi: 10.1074/jbc.TM118.004165.

[6] D. te Vruchte *et al.*, "Accumulation of glycosphingolipids in Niemann-Pick C disease disrupts endosomal transport," *J. Biol. Chem.*, vol. 279, no. 25, pp. 26167–26175, Jun. 2004, doi: 10.1074/jbc.M311591200.

[7] M. T. Vanier, "Niemann-Pick disease type C," *Orphanet J. Rare Dis.*, vol. 5, p. 16, Jun. 2010, doi: 10.1186/1750-1172-5-16.

[8] M. Vanier and G. Millat, "Niemann–Pick disease type C," *Clin. Genet.*, vol. 64, no. 4, pp. 269–281, 2003, doi: 10.1034/j.1399-0004.2003.00147.x.

[9] S. K. Loftus *et al.*, "Murine model of Niemann-Pick C disease: mutation in a cholesterol homeostasis gene," *Science*, vol. 277, no. 5323, pp. 232–235, Jul. 1997, doi: 10.1126/science.277.5323.232.

[10] M. Labrecque, L. Touma, C. Bhérer, A. Duquette, and M. Tétreault, "Estimated prevalence of Niemann–Pick type C disease in Quebec," *Sci. Rep.*, vol. 11, no. 1, Art. no. 1, Nov. 2021, doi: 10.1038/s41598-021-01966-0.

[11] J. E. Wraith *et al.*, "Recommendations on the diagnosis and management of Niemann-Pick disease type C," *Mol. Genet. Metab.*, vol. 98, no. 1, pp. 152–165, Oct. 2009, doi: 10.1016/j.ymgme.2009.06.008.

[12] S. U. Walkley and K. Suzuki, "Consequences of NPC1 and NPC2 loss of function in mammalian neurons," *Biochim. Biophys. Acta BBA - Mol. Cell Biol. Lipids*, vol. 1685, no. 1, pp. 48–62, Oct. 2004, doi: 10.1016/j.bbalip.2004.08.011.

[13] J. Newton, S. Milstien, and S. Spiegel, “Niemann-Pick type C disease: The atypical sphingolipidosis,” *Adv. Biol. Regul.*, vol. 70, pp. 82–88, Dec. 2018, doi: 10.1016/j.jbior.2018.08.001.

[14] M. Malnar, S. Hecimovic, N. Mattsson, and H. Zetterberg, “Bidirectional links between Alzheimer’s disease and Niemann-Pick type C disease,” *Neurobiol. Dis.*, vol. 72 Pt A, pp. 37–47, Dec. 2014, doi: 10.1016/j.nbd.2014.05.033.

[15] Y. Sakiyama, A. Narita, S. Osawa, E. Nanba, K. Ohno, and M. Otsuka, “Abnormal copper metabolism in Niemann–Pick disease type C mimicking Wilson’s disease,” *Neurol. Clin. Neurosci.*, vol. 2, no. 6, pp. 193–200, 2014, doi: 10.1111/ncn3.122.

[16] S. Grassi *et al.*, “Sphingosine 1-Phosphate Receptors and Metabolic Enzymes as Druggable Targets for Brain Diseases,” *Front. Pharmacol.*, vol. 10, 2019, Accessed: Jul. 07, 2022. [Online]. Available: https://www.frontiersin.org/articles/10.3389/fphar.2019.00807

[17] E. B. Vitner, F. M. Platt, and A. H. Futerman, “Common and Uncommon Pathogenic Cascades in Lysosomal Storage Diseases,” *J. Biol. Chem.*, vol. 285, no. 27, pp. 20423–20427, Jul. 2010, doi: 10.1074/jbc.R110.134452.

[18] J. Newton *et al.*, “Targeting defective sphingosine kinase 1 in Niemann–Pick type C disease with an activator mitigates cholesterol accumulation,” *J. Biol. Chem.*, vol. 295, no. 27, pp. 9121–9133, Jul. 2020, doi: 10.1074/jbc.RA120.012659.

[19] H. Lee *et al.*, “Pathological roles of the VEGF/SphK pathway in Niemann–Pick type C neurons,” *Nat. Commun.*, vol. 5, no. 1, Art. no. 1, Nov. 2014, doi: 10.1038/ncomms6514.

[20] S. Spiegel and S. Milstien, “Sphingosine-1-phosphate: an enigmatic signalling lipid,” *Nat. Rev. Mol. Cell Biol.*, vol. 4, no. 5, Art. no. 5, May 2003, doi: 10.1038/nrm1103.

[21] S. Grassi, E. Chiricozzi, L. Mauri, S. Sonnino, and A. Prinetti, “Sphingolipids and neuronal degeneration in lysosomal storage disorders,” *J. Neurochem.*, vol. 148, no. 5, pp. 600–611, Mar. 2019, doi: 10.1111/jnc.14540.

[22] A. Singh and M. Del Poeta, “Sphingolipidomics: An Important Mechanistic Tool for Studying Fungal Pathogens,” *Front. Microbiol.*, vol. 7, 2016, Accessed: May 23, 2022. [Online]. Available: https://www.frontiersin.org/article/10.3389/fmicb.2016.00501

[23] F. J. Roisen, H. Bartfeld, R. Nagele, and G. Yorke, “Ganglioside stimulation of axonal sprouting in vitro,” *Science*, vol. 214, no. 4520, pp. 577–578, Oct. 1981, doi: 10.1126/science.7291999.

[24] B. M. Quinville, N. M. Deschenes, A. E. Ryckman, and J. S. Walia, “A Comprehensive Review: Sphingolipid Metabolism and Implications of Disruption in Sphingolipid Homeostasis,” *Int. J. Mol. Sci.*, vol. 22, no. 11, p. 5793, May 2021, doi: 10.3390/ijms22115793.

[25] C. Gault, L. Obeid, and Y. Hannun, “An overview of sphingolipid metabolism: from synthesis to breakdown,” *Adv. Exp. Med. Biol.*, vol. 688, pp. 1–23, 2010.

[26] T. A. Taha, T. D. Mullen, and L. M. Obeid, “A house divided: ceramide, sphingosine, and sphingosine-1-phosphate in programmed cell death,” *Biochim. Biophys. Acta*, vol. 1758, no. 12, pp. 2027–2036, Dec. 2006, doi: 10.1016/j.bbamem.2006.10.018.

[27] R. Pralhada Rao, N. Vaidyanathan, M. Rengasamy, A. Mammen Oommen, N. Somaiya, and M. R. Jagannath, “Sphingolipid Metabolic Pathway: An Overview of Major Roles Played in Human Diseases,” *J. Lipids*, vol. 2013, p. e178910, Aug. 2013, doi: 10.1155/2013/178910.

[28] M. Maceyka *et al.*, “SphK1 and SphK2, sphingosine kinase isoenzymes with opposing functions in sphingolipid metabolism,” *J. Biol. Chem.*, vol. 280, no. 44, pp. 37118–37129, Nov. 2005, doi: 10.1074/jbc.M502207200.

[29] Y. A. Hannun, C. Luberto, and K. M. Argraves, “Enzymes of Sphingolipid Metabolism: From Modular to Integrative Signaling,” *Biochemistry*, vol. 40, no. 16, pp. 4893–4903, Apr. 2001, doi: 10.1021/bi002836k.

[30] M. Maceyka and S. Spiegel, “Sphingolipid metabolites in inflammatory disease,” *Nature*, vol. 510, no. 7503, Art. no. 7503, Jun. 2014, doi: 10.1038/nature13475.

[31] F. Bourquin, G. Capitani, and M. G. Grütter, “PLP-dependent enzymes as entry and exit gates of sphingolipid metabolism,” *Protein Sci. Publ. Protein Soc.*, vol. 20, no. 9, pp. 1492–1508, Sep. 2011, doi: 10.1002/pro.679.

[32] J. Newton, S. Lima, M. Maceyka, and S. Spiegel, “Revisiting the sphingolipid rheostat: evolving concepts in cancer therapy,” *Exp. Cell Res.*, vol. 333, no. 2, pp. 195–200, May 2015, doi: 10.1016/j.yexcr.2015.02.025.

[33] K. Kitatani, J. Idkowiak-Baldys, and Y. A. Hannun, “The sphingolipid salvage pathway in ceramide metabolism and signaling,” *Cell. Signal.*, vol. 20, no. 6, pp. 1010–1018, Jun. 2008, doi: 10.1016/j.cellsig.2007.12.006.

[34] B. K. Gillard, R. G. Clement, and D. M. Marcus, “Variations among cell lines in the synthesis of sphingolipids in de novo and recycling pathways,” *Glycobiology*, vol. 8, no. 9, pp. 885–890, Sep. 1998, doi: 10.1093/glycob/8.9.885.

[35] G. Tettamanti, R. Bassi, P. Viani, and L. Riboni, “Salvage pathways in glycosphingolipid metabolism,” *Biochimie*, vol. 85, no. 3–4, pp. 423–437, Apr. 2003, doi: 10.1016/s0300-9084(03)00047-6.

[36] J. Qin, E. Berdyshev, J. Goya, V. Natarajan, and G. Dawson, “Neurons and Oligodendrocytes Recycle Sphingosine 1-Phosphate to Ceramide,” *J. Biol. Chem.*, vol. 285, no. 19, pp. 14134–14143, May 2010, doi: 10.1074/jbc.M109.076810.

[37] M. Maceyka, K. B. Harikumar, S. Milstien, and S. Spiegel, “Sphingosine-1-phosphate signaling and its role in disease,” *Trends Cell Biol.*, vol. 22, no. 1, pp. 50–60, Jan. 2012, doi: 10.1016/j.tcb.2011.09.003.

[38] T. Hla, “Physiological and pathological actions of sphingosine 1-phosphate,” *Semin. Cell Dev. Biol.*, vol. 15, no. 5, pp. 513–520, Oct. 2004, doi: 10.1016/j.semcdb.2004.05.002.

[39] T. A. Taha, Y. A. Hannun, and L. M. Obeid, “Sphingosine Kinase: Biochemical and Cellular Regulation and Role in Disease,” *BMB Rep.*, vol. 39, no. 2, pp. 113–131, 2006, doi: 10.5483/BMBRep.2006.39.2.113.

[40] J. Liu, B. S. Beckman, and M. Foroozesh, “A review of ceramide analogs as potential anticancer agents,” *Future Med. Chem.*, vol. 5, no. 12, pp. 1405–1421, Aug. 2013, doi: 10.4155/fmc.13.107.

[41] E. Wang, X. He, and M. Zeng, “The Role of S1P and the Related Signaling Pathway in the Development of Tissue Fibrosis,” *Front. Pharmacol.*, vol. 9, 2019, Accessed: May 23, 2022. [Online]. Available: https://www.frontiersin.org/article/10.3389/fphar.2018.01504

[42] P. Xia *et al.*, “Sphingosine kinase interacts with TRAF2 and dissects tumor necrosis factor-alpha signaling,” *J. Biol. Chem.*, vol. 277, no. 10, pp. 7996–8003, Mar. 2002, doi: 10.1074/jbc.M111423200.

[43] S. E. Alvarez *et al.*, “Sphingosine-1-phosphate is a missing cofactor for the E3 ubiquitin ligase TRAF2,” *Nature*, vol. 465, no. 7301, Art. no. 7301, Jun. 2010, doi: 10.1038/nature09128.

[44] T. Liu, L. Zhang, D. Joo, and S.-C. Sun, “NF-κB signaling in inflammation,” *Signal Transduct. Target. Ther.*, vol. 2, no. 1, Art. no. 1, Jul. 2017, doi: 10.1038/sigtrans.2017.23.

[45] A. Lucaciu, R. Brunkhorst, J. M. Pfeilschifter, W. Pfeilschifter, and J. Subburayalu, “The S1P–S1PR Axis in Neurological Disorders—Insights into Current and Future Therapeutic Perspectives,” *Cells*, vol. 9, no. 6, Art. no. 6, Jun. 2020, doi: 10.3390/cells9061515.

[46] K. Takabe, S. W. Paugh, S. Milstien, and S. Spiegel, “‘Inside-out’ signaling of sphingosine-1-phosphate: therapeutic targets,” *Pharmacol. Rev.*, vol. 60, no. 2, pp. 181–195, Jun. 2008, doi: 10.1124/pr.107.07113.

[47] M. Nagahashi *et al.*, “Sphingosine-1-Phosphate Transporters as Targets for Cancer Therapy,” *BioMed Res. Int.*, vol. 2014, p. 651727, 2014, doi: 10.1155/2014/651727.

[48] S. Pyne, D. R. Adams, and N. J. Pyne, “Sphingosine 1-phosphate and sphingosine kinases in health and disease: Recent advances,” *Prog. Lipid Res.*, vol. 62, pp. 93–106, Apr. 2016, doi: 10.1016/j.plipres.2016.03.001.

[49] S. Spiegel and S. Milstien, “The outs and the ins of sphingosine-1-phosphate in immunity,” *Nat. Rev. Immunol.*, vol. 11, no. 6, pp. 403–415, Jun. 2011, doi: 10.1038/nri2974.

[50] Y. Okamoto, F. Wang, K. Yoshioka, N. Takuwa, and Y. Takuwa, “Sphingosine-1-Phosphate-Specific G Protein-Coupled Receptors as Novel Therapeutic Targets for Atherosclerosis,” *Pharmaceuticals*, vol. 4, no. 1, Art. no. 1, Jan. 2011, doi: 10.3390/ph4010117.

[51] G. T. Kunkel, M. Maceyka, S. Milstien, and S. Spiegel, “Targeting the sphingosine-1-phosphate axis in cancer, inflammation and beyond,” *Nat. Rev. Drug Discov.*, vol. 12, no. 9, pp. 688–702, Sep. 2013, doi: 10.1038/nrd4099.

[52] V. A. Blaho and T. Hla, “An update on the biology of sphingosine 1-phosphate receptors,” *J. Lipid Res.*, vol. 55, no. 8, pp. 1596–1608, Aug. 2014, doi: 10.1194/jlr.R046300.

[53] R. L. Proia and T. Hla, “Emerging biology of sphingosine-1-phosphate: its role in pathogenesis and therapy,” *J. Clin. Invest.*, vol. 125, no. 4, pp. 1379–1387, Apr. 2015, doi: 10.1172/JCI76369.

[54] Y. Yuan *et al.*, “Structures of signaling complexes of lipid receptors S1PR1 and S1PR5 reveal mechanisms of activation and drug recognition,” *Cell Res.*, vol. 31, no. 12, Art. no. 12, Dec. 2021, doi: 10.1038/s41422-021-00566-x.

[55] M. Hoque *et al.*, “The cross-talk of LDL-cholesterol with cell motility: insights from the Niemann Pick Type C1 mutation and altered integrin trafficking,” *Cell Adhes. Migr.*, vol. 9, no. 5, pp. 384–391, 2015, doi: 10.1080/19336918.2015.1019996.

[56] T. Bialistoky *et al.*, “Functional analysis of Niemann-Pick disease type C family protein, NPC1a, in Drosophila melanogaster,” *Development*, vol. 146, no. 10, p. dev168427, May 2019, doi: 10.1242/dev.168427.

[57] S. Lima, S. Milstien, and S. Spiegel, “Sphingosine and Sphingosine Kinase 1 Involvement in Endocytic Membrane Trafficking,” *J. Biol. Chem.*, vol. 292, no. 8, pp. 3074–3088, Feb. 2017, doi: 10.1074/jbc.M116.762377.

[58] M. M. Young, Y. Takahashi, T. E. Fox, J. K. Yun, M. Kester, and H.-G. Wang, “Sphingosine Kinase 1 Cooperates with Autophagy to Maintain Endocytic Membrane Trafficking,” *Cell Rep.*, vol. 17, no. 6, pp. 1532–1545, Nov. 2016, doi: 10.1016/j.celrep.2016.10.019.

[59] A. Cartier and T. Hla, “Sphingosine 1-phosphate: lipid signaling in pathology and therapy,” *Science*, vol. 366, no. 6463, p. eaar5551, Oct. 2019, doi: 10.1126/science.aar5551.

[60] A. K. Tharkeshwar *et al.*, “A novel approach to analyze lysosomal dysfunctions through subcellular proteomics and lipidomics: the case of NPC1 deficiency,” *Sci. Rep.*, vol. 7, no. 1, Art. no. 1, Jan. 2017, doi: 10.1038/srep41408.

[61] D. Höglinger *et al.*, “NPC1 regulates ER contacts with endocytic organelles to mediate cholesterol egress,” *Nat. Commun.*, vol. 10, no. 1, Art. no. 1, Sep. 2019, doi: 10.1038/s41467-019-12152-2.

[62] M. Praggastis *et al.*, “A Murine Niemann-Pick C1 I1061T Knock-In Model Recapitulates the Pathological Features of the Most Prevalent Human Disease Allele,” *J. Neurosci.*, vol. 35, no. 21, pp. 8091–8106, May 2015, doi: 10.1523/JNEUROSCI.4173-14.2015.

[63] K. J. Livak and T. D. Schmittgen, “Analysis of Relative Gene Expression Data Using Real-Time Quantitative PCR and the 2−ΔΔCT Method,” *Methods*, vol. 25, no. 4, pp. 402–408, Dec. 2001, doi: 10.1006/meth.2001.1262.

[64] M. M. Bradford, “A rapid and sensitive method for the quantitation of microgram quantities of protein utilizing the principle of protein-dye binding,” *Anal. Biochem.*, vol. 72, no. 1, pp. 248–254, May 1976, doi: 10.1016/0003-2697(76)90527-3.

[65] J. Ye, G. Coulouris, I. Zaretskaya, I. Cutcutache, S. Rozen, and T. L. Madden, “Primer-BLAST: A tool to design target-specific primers for polymerase chain reaction,” *BMC Bioinformatics*, vol. 13, p. 134, Jun. 2012, doi: 10.1186/1471-2105-13-134.

[66] “Tissue expression of S1PR5 - Summary - The Human Protein Atlas.” https://www.proteinatlas.org/ENSG00000180739-S1PR5/tissue (accessed Feb. 17, 2023).

[67] W. Liu, B. Liu, S. Liu, J. Zhang, and S. Lin, “Sphingosine-1-phosphate receptor 2 mediates endothelial cells dysfunction by PI3K-Akt pathway under high glucose condition,” *Eur. J. Pharmacol.*, vol. 776, pp. 19–25, Apr. 2016, doi: 10.1016/j.ejphar.2016.02.056.